UCLouvain

epl

École polytechnique de Louvain

Development of a sensor dedicated to the control of a two-degree-of-freedom permanent magnet actuator

Author: **Adrien ALEXANDRE**
Supervisor: **Bruno DEHEZ**
Readers: **Laurent FRANCIS, Guillaume FRANCOIS**
Academic year 2020–2021
Master [120] in Electro-mechanical Engineering

Abstract

For several years now, robots are more and more used for industrial applications and manufacturers are therefore always looking for faster, lighter and more accurate robots. In this context of improvement, L. Body and M. Van Essche worked 2 years ago on the realization of a two-degree-of-freedom permanent magnet actuator. Even if they came up with an impressive prototype, to be able to control such an actuator, an adapted position sensor is needed. The goal of this master's thesis will therefore be the development of a sensor dedicated to the control of this actuator and more generally to the control of two-degree-of-freedom actuators capable of both radial and axial displacements. This paper will therefore describe the development of a capacitive sensor prototype from its initial concept to its experimental testing. The behaviour of this sensor will be studied through the use of an analytical model and validated using a finite element method approach.

Acknowledgements

First and foremost, I would like to thank my supervisor, Pf. Bruno Dehez for his support throughout this academic year. This master's thesis would have never been accomplished without his assistance and advices through the multiple meetings that have been regularly planned.

I would also like to thank Pf. Laurent Francis and Guillaume Francois for being members of my jury and readers of this paper.

I am also grateful to Thierry Daras for his reactivity and availability for the placed orders in the context of this paper.

I would also like to thank Souley Djadjandi and Joachim Van Verdeghem for lending me electrical and mechanical parts used for the realisation of this project.

Finally, I would like to thank all my friends and my family for the support, encouragements and for taking time listening to me when it was needed.

Contents

Introduction

For several years now, robotics has become more and more present in our society and robots are used in many fields. Whether being for industrial, military, medical or even for domestic or leisure applications, there are thousands of different kinds of robots and manufacturers are always looking for more accurate, more efficient and faster robots. A track to be studied in this optic of improvement is the number of actuators present on a robot. Indeed, most robots have always been equipped with as many actuators as they have degrees of freedom. Let's take the example of the SCARA robots: they are very common in the industry to perform "pick and place" tasks in production lines.

(a) SCARA robot on a production line

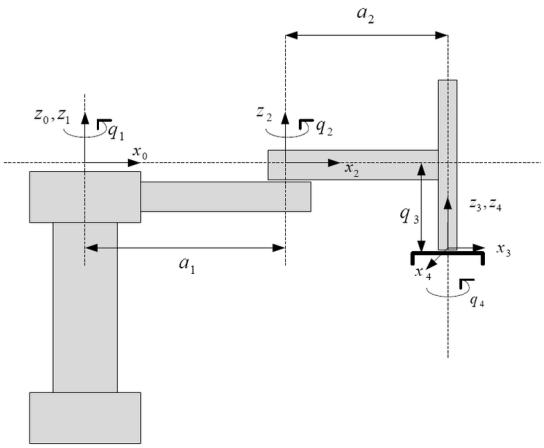

(b) Joints scheme of a SCARA robot

Those robots are composed of 3 revolute joints terminated by a prismatic joint allowing the end effector of the robot to pick an object and replace it in the desired angular position. As mentioned earlier, in order to perform this manipulation, the end effector needs to be actuated by two differents actuators working in series. A way to improve the operation of this type of robot would be to replace the two final actuators by a single actuator that would combine the motion of the other two. In this perspective, two years ago, two students from UCLouvain L. Body and

M. Van Essche worked on the development of a two-degree-of-freedom permanent magnet actuator and they came up with the following prototype :

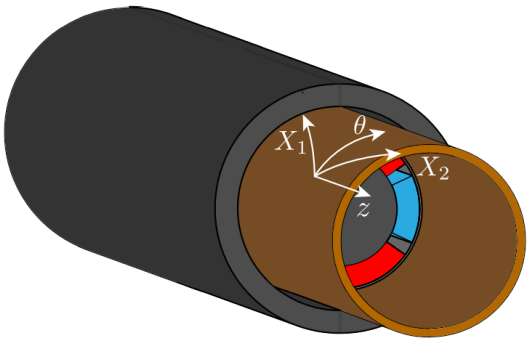

(a) Actuator prototype

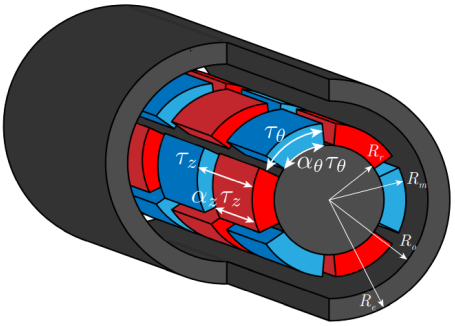

(b) Stator's permanent magnets disposition

It is made up of two parts :

- A rotor made of a flexible PCB containing a copper winding.
- A stator made of an alternation of permanent magnets with inverted polarity.

The disposition of the permanent magnets and the specific layout of the copper wiring allows the rotor to move radially and/or axially depending on the voltage applied on the rotor. The main dimensions of this prototype are the following :

- PCB outer radius : 11.8 [mm]
- PCB inner radius : 10.3 [mm]
- PCB axial length : 75 [mm]
- Back-iron inner radius : 12.3 [mm]
- Permanent magnets outer radius : 9.15 [mm]

Now in order to control the position of the end effector of a robot, sensors are used on the different actuators to have a feedback on their positions. There are many types of sensors capable of measuring various phenomena such as pression, distances, forces, magnetic fields, displacements and many others. To do so, they are based on different technologies depending on what they are used for. There are for example capacitive sensors, inductive sensors, resistive sensors, optical sensors all having several application fields.

In the case of robotics applications, displacement sensors are used on the different actuators to measure both radial or linear displacement. The challenge when using an actuator that combines both motions is thus to use a sensor that is also capable of measuring both positions at the same time. As this technology of actuator is not yet widespread, it is difficult to find sensors meeting those requirements. The purpose of this master's thesis will therefore be the implementation and the validation of a sensor capable of measuring both a radial and axial displacement at the same time.

In the context of the appliaction of this sensor to the prototype presented above, a requirements specification was drawn up resuming the various characteristics this sensor will have to respect.

Requirements specification table	
Absolute sensor only	
Contactless and wireless sensor	
Linear range of working	8 [cm]
Angular range of working	360 [°]
Absolute linear error	< 0.5 %
Absolute angular error	< 0.5 %
Linear resolution	1 [mm]
Angular resolution	5 [°]

Table 1: Requirements specification table

It has been decided to only consider the development of absolute sensors : as it could be used in industrial applications, this would allow not to have to reset the sensor when being subject to power cut for example. This sensor also has to be contactless and wireless in order to avoid friction or obstruction with the rotor. Then the linear range of working has been fixed based on the PCB axial length of 7.5 [cm]. The resolution have been set to 1 [mm] and 5 [°] as it represents approximately 1 % of the working range. Finally, the absolute maximum error has been fixed to 0.5 % according to typical values found on sensor's datasheets.

Chapter 1

Sensors design

As a first step, different solutions based on various technologies have been imagined. As they had to fulfill the requirements and be adaptable to the concerned actuator, 2 main solutions have been retained : one based on a capacitive measure and the other based on a coded position sensor. This chapter will thus review those 2 main designed prototypes with their strenghts and weaknesses and conclude by choosing the sensor that will be studied in this paper.

1.1 Capacitive sensor

Capacitive sensors are a widely used type of sensor and they can be found in several applications of the daily life like the measurement of pressure, position, displacement, force, humidity, fluid level, acceleration and many others. Looking at the general formula of a cylindrical capacitance brings the different parameters that can be studied in order to be able to measure a position.

$$C = \frac{\epsilon_r \epsilon_0 \theta l}{ln(\frac{R_b}{R_a})} \tag{1.1}$$

With :

- θl : the facing area between the inner and outer electrode of the capacitance with θ and L respectively the angle and length of the facing area.
- R_b,R_a : the inner and outer radius of the capacitance.
- ϵ_r : the relative permittivity of the dielectric between the electrodes.

By choosing the facing area as the sensing parameter, the following prototype has been designed :

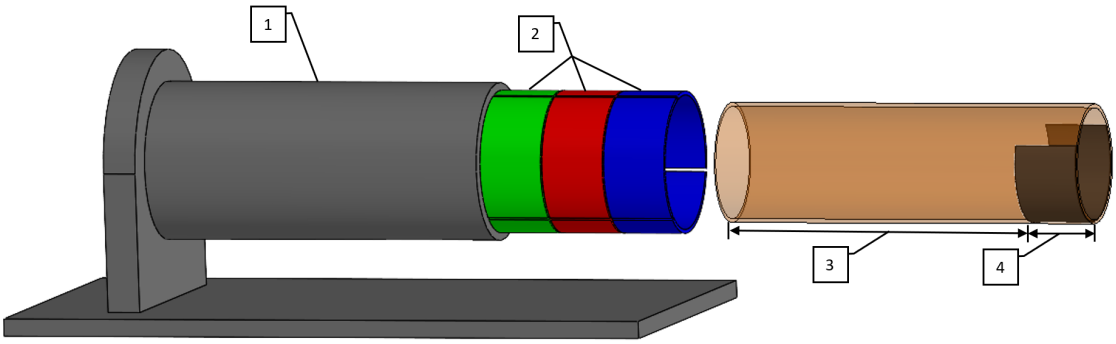

Figure 1.1: General view of the capacitive sensor mounted on the original motor

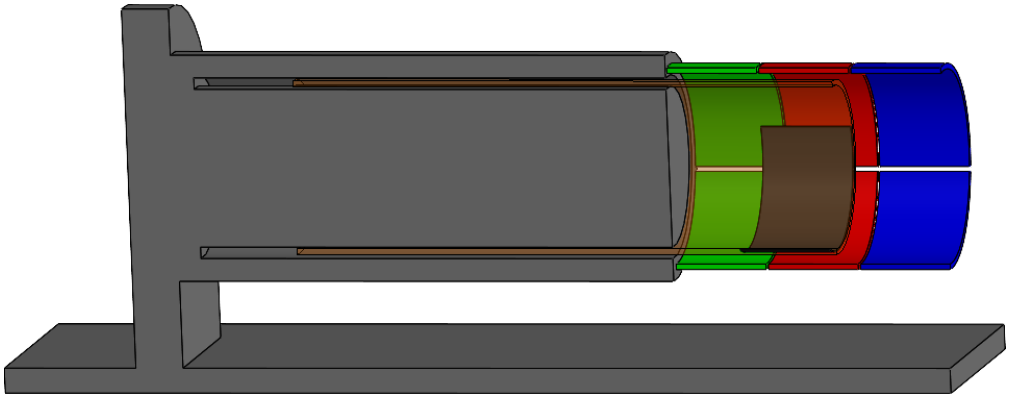

Figure 1.2: Section view of the capacitive sensor mounted on the original sensor

This prototype is composed of 4 differents parts :

- The original stator with its permanent magnets (1).
- N triplets of electrodes that are fixed at the stator extremity (2). In this example, N=3. One triplet of electrode is composed of 3 electrodes with an angle of revolution of $\frac{2\pi}{3}$ and a width depending on the number of triplets and the desired measuring range.
- The original rotor is composed of a flexible PCB with the winding (3) and has been extended in order to place an electrode in it (4). This electrode has the same width as one triplet of electrode and an angle of revolution of $\frac{4\pi}{3}$.

This sensor works as follows :
In each triplet of electrode, the 3 different capacitances made between 2 of the 3 outer electrodes are measured alternatly. Because the rotor's electrode has the same width as one triplet of electrode it can therefore not be facing every triplet (it will be facing 1 of them or be between 2 of them). This is why 2 cases will be distinguished :

- If the rotor's electrode is facing the triplet, the measurement will return 3 different capacitances that are in fact the serialization of 2 capacitances made between the rotor's electrode and the 2 outer electrodes.

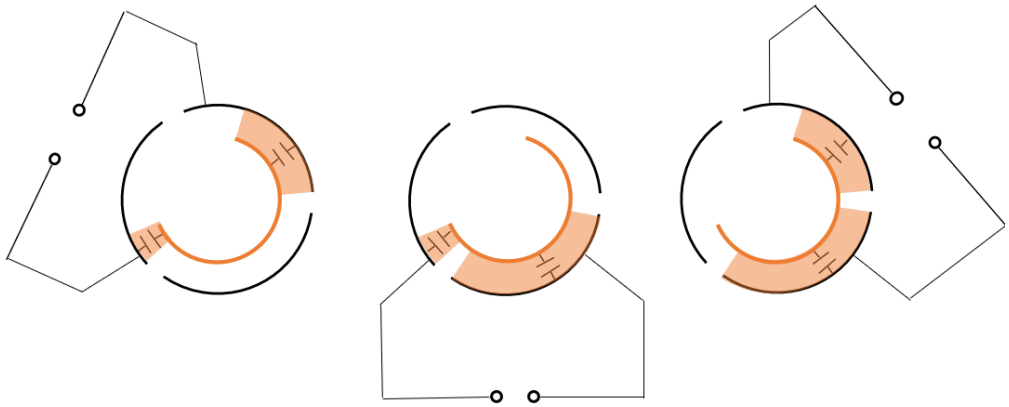

Figure 1.3: Measuring method of the capacitances inside a triplet of electrodes

- If the rotor's electrode is not facing the triplet, the 3 capacitances will simply be equal to zero (if we neglect the parasitic capacitances).

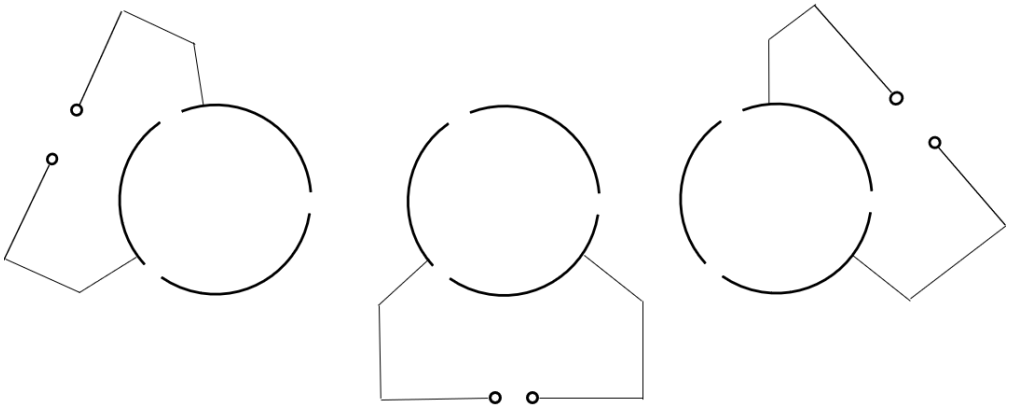

Figure 1.4: Measuring method of the capacitances inside a triplet of electrodes

The value of the 3 measured capacitances inside the triplet which has the most facing area with the rotor's electrode will be used in order to determine the radial position. Then, the comparison of the sum of the 3 capacitances measured at the 2 triplets between which the rotor's electrode straddles will be used to determine the axial position.

Advantages	Disadvantages
As the flexible PCB of the rotor already exists, the electrode can simply be added in the manufacturing process.	The total width of the fixed electrodes depends on the measurement range and can therefore be relatively spacious.
Capable of measuring large range of values	Low response time for large number of triplets N as many capacitances have to be measured.

1.2 Coded position sensor

Coded position senors are mainly used to determine angular or linear positions. They are composed of a light source (photoemitter) and a photoreceiver. The light sent by the photoemitter passes through an alternating opaque and translucent grid so that the light reaching (or not) the photoreceiver provides a digital information of the actuator's position.

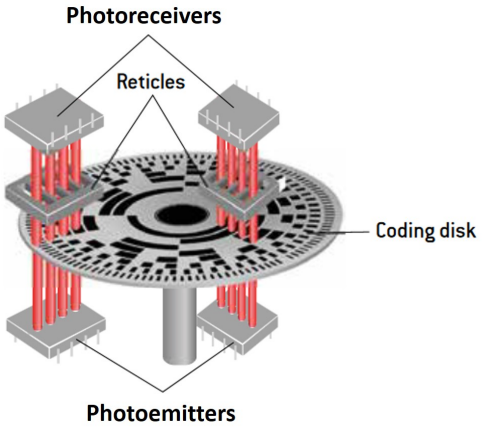

(a) Absolute angular encoder

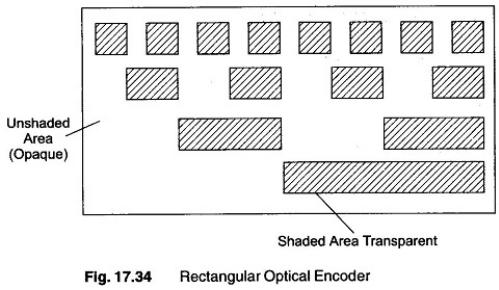

Fig. 17.34 Rectangular Optical Encoder

(b) Linear encoder pattern

The challenge of a sensor for the studied application would be to store both the radial and axial position into a single binary information. To do so, the concept of the De Bruijn sequence will be used. A De Bruijn sequence of order n on a size-k alphabet A is a cyclic sequence in which every possible length-n string on A occurs exactly once as a substring.

For example, by taking an alphabet of size k=2 (as the encoder only considers the 0 or 1 value) and an order n=4, the following sequence is obtained :

$$0000100110101111000 \tag{1.2}$$

Taking 4 consecutives values in this sequence will thus never give 2 times the same sub-sequence and it is possible to find k^n differents sub-sequences of n values. This concept could be used to design a linear encoder where the shifting of this sequence to the right or to the left means a displacement of x [mm] and to be able to read up to $k^n = 16$ positions, with n the number of photoemitters :

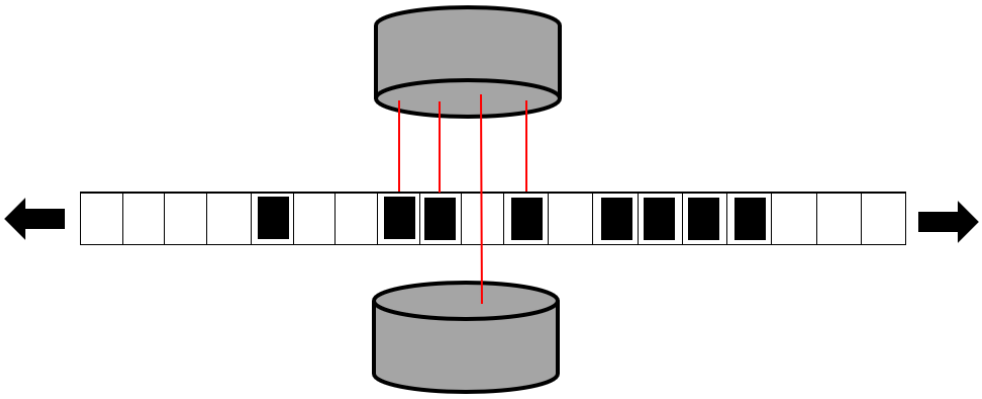

Figure 1.6: Linear encoder sensor using the De Bruijn sequence

Now bringing this sequence into a 2-dimensional sequence would allow to sense a displacement in 2 directions :

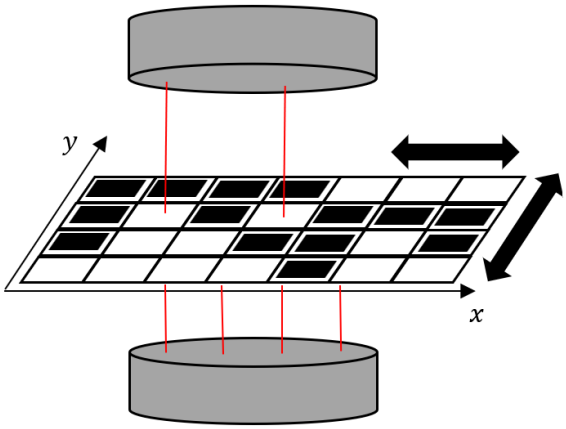

y_4	1111	1110	1100	1000
y_3	1010	0101	1011	0111
y_2	1001	0011	1001	1101
y_1	0000	0001	0010	0100
/	x_1	x_2	x_3	x_4

Table 1.2: Readed sequence for a given position

Table 1.1: 2-dimensions encoder sensor

Where it is possible to sense up to i positions in the x-direction and j positions in the y-direction by respecting $ij \leq k^n$. In this example, $i = j = 4$.

Finally, by bringing the 2-dimension cartesian frame into a cylindrical frame, the following prototype has been developped :

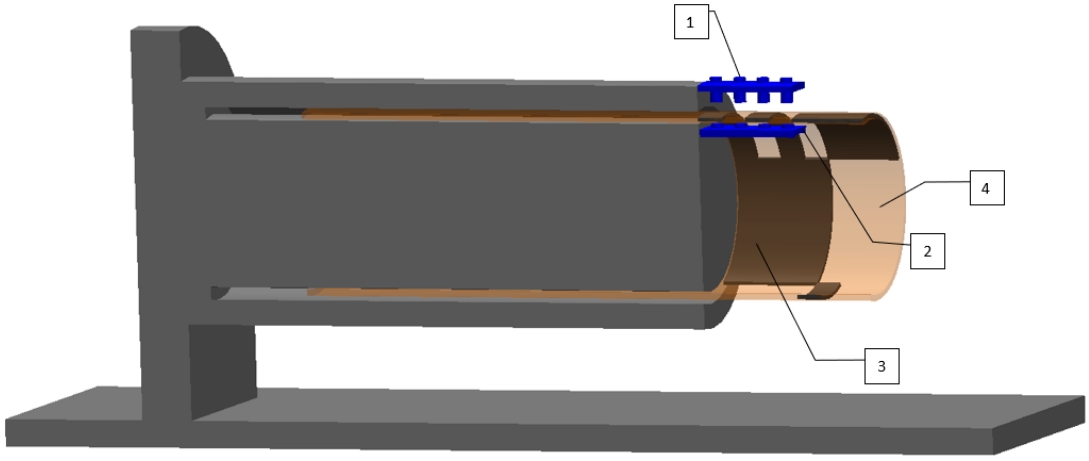

Figure 1.7: Cylindrical encoder prototype

It is made up of photoemitters (1) and photoreceivers (2) which have been added at the end of the stator. Copper zones (3) have been added into the flexible PCB (4) in order to act as the opaque and translucent grid. Here's a zoom on the cylindrical grid used in this sensor :

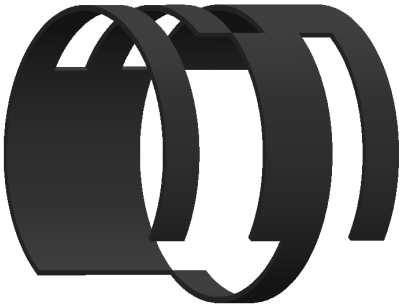

Figure 1.8: Cylindrical grid

As mentionned earlier, this configuration allows to sense 4 positions in each directions which means a resolution of $\frac{360°}{4} = 90°$ in the radial direction and a resolution of $\frac{1}{4}^{th}$ of the working range in the axial direction. Now, to be able to reach the desired resolution (5[°] and 1 [mm] for a working range of 8 [cm]),$ij = 5760$ different measured positions would be needed. By respecting $ij \leq k^n$, this means that at least 13 photoemitters would be required.

Advantages	Disadvantages
Facility of implementation.	High number of photoemitter and photoreceiver needed in order to reach an high accuracy.

1.3 Choice of the sensor

As a large number of photoemitters would be needed in order to reach the desired resolution and as the coded position sensor is limited to relatively small working ranges, it has been decided to study more deeply the capacitive sensor. Indeed this solution offers more flexibility and could therefore be easily adapted to similar actuators.

Chapter 2

Sensor analytical modelling

In this chapter, the selected capacitive solution introduced in the previous section will be studied more specifically by looking closer to the functioning principle of this sensor and analyse the variations caused by the modification of the different parameters of this model.

2.1 Parameters, notations and positionning references

Before going further, here's a view of the different parameters of the sensor and the notation that go along with it. The electrodes fixed to the stator will be numbered from 1 to N and more precisely from 1 to 3 for the 1^{st} triplet, 4 to 6 for the 2^{nd} triplet and from 3N-2 to 3N for the N^{th} triplet as shown on figure 2.1.

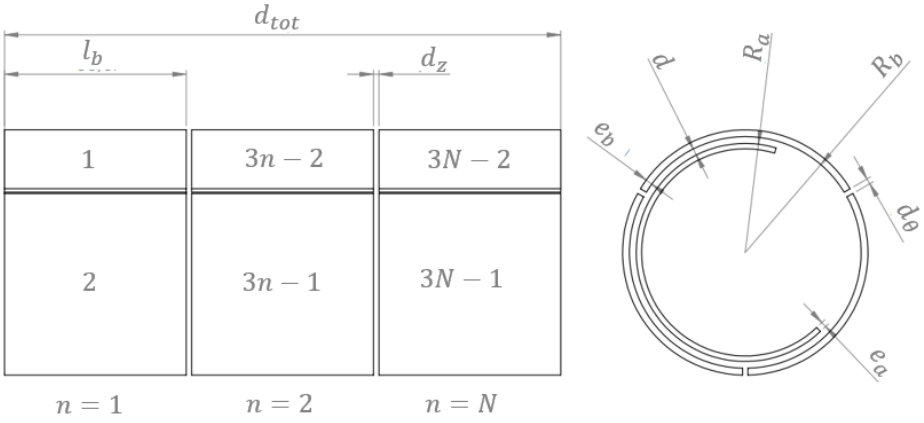

Figure 2.1: Parameters of the sensor

With :

- l_b : The width of an outer electrode
- l_a : The width of the inner electrode
- d_{tot} : The total width
- d_z : The axial distance between two electrodes
- N : The number of triplet of electrodes
- e_b : The thickness of an outer electrode
- d : The distance between the inner and outer electrodes
- R_a : The radius of the inner electrode
- R_b : The radius of the outer electrode
- d_θ : The radial distance between two electrodes
- e_a : The thickness of an inner electrode
- Δ_z = The axial working range of the sensor
- Δ_θ = The radial working range of the sensor

Then, the following reference frames will be used :

- $\{x_s, y_s, z_s\}$: the reference frame of the stator with the origin placed on the axis of revolution in the middle of the N triplets set, z_s aligned with the axis of revolution and x_s pointing to the extremity of the 1^{st} electrode of each triplet.
- $\{x_r, y_r, z_r\}$: the reference frame of the rotor with the origin placed on the axis of revolution in the middle of the rotor's electrode, z_r aligned with the axis of revolution and x_r pointing to the extremity of the rotor's electrode.

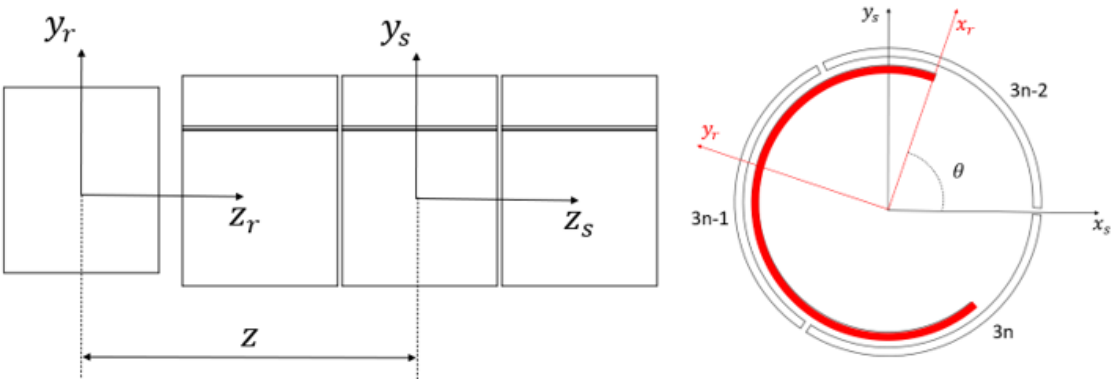

Figure 2.2: Reference frame of the stator and rotor

The position of the rotor will then be defined as $[z; \theta]$.
With :

- z: The distance between both origins in the range $\Delta_z = [-\frac{d_{tot}}{2} + \frac{l_a}{2}; \frac{d_{tot}}{2} - \frac{l_a}{2}]$
- θ : the angle between x_r and x_s in the range $\Delta_\theta = [0; 2\pi]$

As regards the different capacitances, the following conventions will be used in this document :

- C_n corresponds to the capacitance between the n^{th} electrode of the stator and the rotor's electrode.
- $C_{i,j}$ corresponds to the capacitance between 2 outer electrodes (the i^{th} and j^{th} electrode) and is the serialization of C_i and C_j.

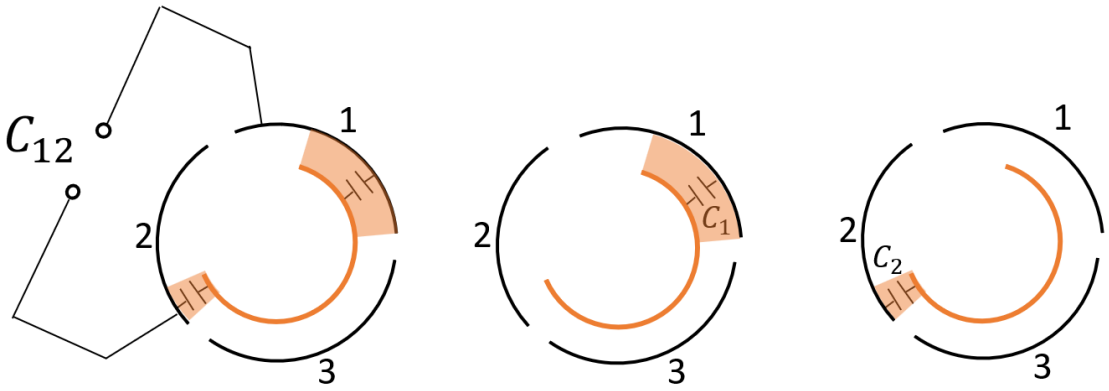

Figure 2.3: Capacitances notation conventions

2.2 Basic case

Now that all the conventions have been fixed the behaviour of the sensor will be studied with an ideal case by making the following simplifications and hypotheses :

- All the outer electrodes are close to each other :
  - $d_\theta = 0$
  - $d_z = 0$
- The inner and outer electrode have the same width : $l_a = l_b$
- We have no parasitic capacitances
- Air is present between the electrodes : $\epsilon_r = 1$
- The thickness of all the electrodes is equal to zero $e_a = e_b = 0$
- The capacitance C_n is computed by using the general formula of a cylindrical capacitance : $C = \frac{\epsilon_r \epsilon_0 \theta l}{ln(\frac{R_b}{R_a})}$ with θ and l respectively the angle and length of the facing area between the electrodes and the capacitance $C_{i,j}$ is thus computed by using the formula of 2 capacitances in series : $C_{i,j} = (\frac{1}{C_i} + \frac{1}{C_j})^{-1}$.

2.2.1 Reverse function

Before being able to design an algorithm that retrieves the position of the sensor for a given set of values of capacitances, a reverse function that gives the values of the different capacitances for a given position had to be implemented. This function will then be used to plot the shape of the different graphs according to a displacement of this sensor in the 2 directions. After specifying all the desired parameters, it will thus return a 3xN matrix with the value of all the capacitances based on the formula of the cylindrical capacitance :

$$f(\theta, z) = \begin{pmatrix} C_1 & C_{3n-2} & ... & C_{3N-2} \\ C_2 & C_{3n-1} & ... & C_{3N-1} \\ C_3 & C_{3n} & ... & C_{3N} \end{pmatrix} \tag{2.1}$$

Here's a graphic example of the functioning of this function :

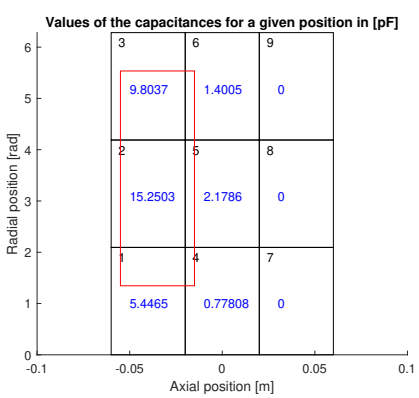

(a) $N = 3, \theta = \frac{3\pi}{7}[rad], z = -0.035[m]$

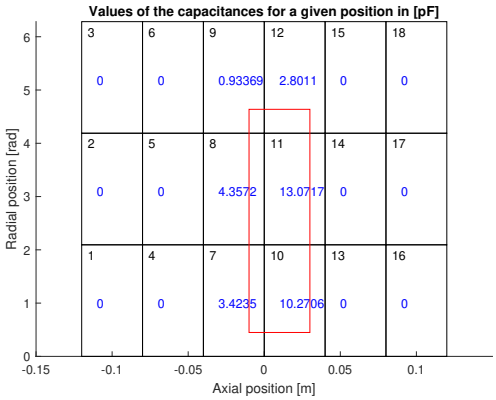

(b) $N = 6, \theta = \frac{\pi}{7}[rad], z = 0.01[m]$

Figure 2.4: $l_a = l_b = 4[cm], R_A = 11.5[mm], R_B = 12[mm]$

As the only variables that will be measured are the values of the capacitances $C_{i,j}$ between 2 outer electrodes. The function will therefore finally compute :

$$f\left(\begin{pmatrix} C_1 & C_{3n-2} & \dots & C_{3N-2} \\ C_2 & C_{3n-1} & \dots & C_{3N-1} \\ C_3 & C_{3n} & \dots & C_{3N} \end{pmatrix}\right) = \begin{pmatrix} C_{1,2} & C_{3n-2,3n-1} & \dots & C_{3N-2,3N-1} \\ C_{1,3} & C_{3n-2,3n} & \dots & C_{3N-2,3N} \\ C_{2,3} & C_{3n-1,3n} & \dots & C_{3N-1,3N} \end{pmatrix} \tag{2.2}$$

Using this function, the following graphs have been plotted :

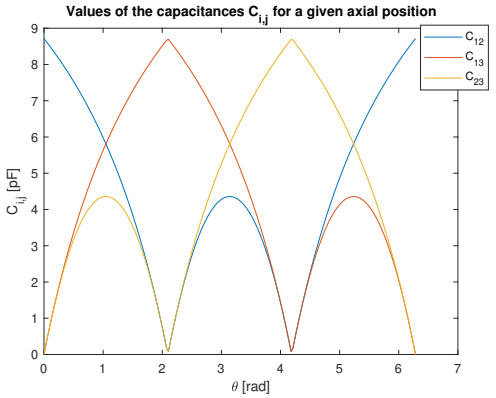

(a) Values of the capacitances $C_{i,j}$ for $z = -0.04$ $[m]$ and for $\theta = [0, 2\pi]$ $[rad]$

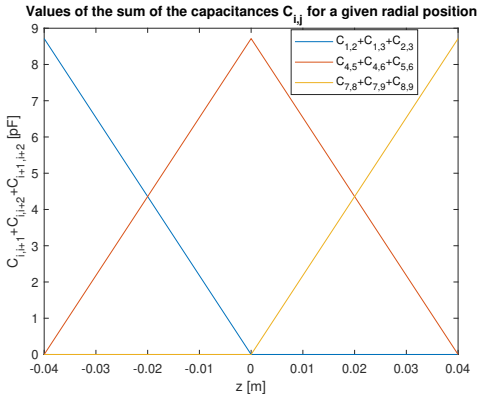

(b) Values of the sum of the capacitances $C_{i,i+1} + C_{i,i+2} + C_{i+1,i+2}$ for $\theta = 0$ $[rad]$ and for $z = [-0.04, 0.04]$ $[m]$

Figure 2.5: $N = 3, l_a = l_b = 4[cm], R_A = 11.5[mm], R_B = 12[mm]$

As the graph of an axial displacement of the rotor's electrode is linear, it should be easy to analyze the different capacitances in order to retrieve the axial postion. The

problem comes from the graph of the radial displacement that is a 2^d degree polynom characteristic. However, by looking at the formula of a cylindrical capacitance, the shape of the graph of the capacitances C_i should be linear for a fixed z position. It would therefore be useful to be able to compute the value of a capacitance C_i from the values of the capacitances $C_{i,j}$.

2.2.2 Finding C_i from $C_{i,j}$

As a reminder the formula of two capacitances in series is:

$$C_{i,j} = (\frac{1}{C_i} + \frac{1}{C_j})^{-1} \tag{2.3}$$

Using this formula in the 1^{st} triplet will lead to the following system :

$$\begin{cases} C_{1,2} = \frac{1}{\frac{1}{C_1}+\frac{1}{C_2}} \\ C_{2,3} = \frac{1}{\frac{1}{C_2}+\frac{1}{C_3}} \\ C_{1,3} = \frac{1}{\frac{1}{C_1}+\frac{1}{C_3}} \end{cases} \tag{2.4}$$

As this is a system of 3 equations with 3 unknowns, it is possible by using substitution to isolate the 3 unknowns C_1, C_2 and C_3 :

$$C_1 = \frac{2C_{1,2}C_{2,3}C_{1,3}}{C_{2,3}C_{1,3} - C_{1,2}C_{1,3} + C_{2,3}C_{1,2}} \tag{2.5}$$

$$C_2 = \frac{2C_{1,2}C_{2,3}C_{1,3}}{C_{2,3}C_{1,3} + C_{1,2}C_{1,3} - C_{2,3}C_{1,2}} \tag{2.6}$$

$$C_3 = \frac{2C_{1,2}C_{2,3}C_{1,3}}{-C_{2,3}C_{1,3} + C_{1,2}C_{1,3} + C_{2,3}C_{1,2}} \tag{2.7}$$

This concept can then be extended to the other triplets to isolate every capacitances C_i.

2.2.3 Functioning of the algorithm

The purpose of the algorithm is to retrieve the position of the sensor with as only input, the matrix of the capacitances $C_{i,j}$:

$$f(\begin{pmatrix} C_{1,2} & C_{3n-2,3n-1} & ... & C_{3N-2,3N-1} \\ C_{1,3} & C_{3n-2,3n} & ... & C_{3N-2,3N} \\ C_{2,3} & C_{3n-1,3n} & ... & C_{3N-1,3N} \end{pmatrix}) = (\theta, z) \tag{2.8}$$

The first step, as explained in the previous section, will therefore be to compute the value of the capacitances C_i:

$$f(\begin{pmatrix} C_{1,2} & C_{3n-2,3n-1} & ... & C_{3N-2,3N-1} \\ C_{1,3} & C_{3n-2,3n} & ... & C_{3N-2,3N} \\ C_{2,3} & C_{3n-1,3n} & ... & C_{3N-1,3N} \end{pmatrix}) = \begin{pmatrix} C_1 & C_{3n-2} & ... & C_{3N-2} \\ C_2 & C_{3n-1} & ... & C_{3N-1} \\ C_3 & C_{3n} & ... & C_{3N} \end{pmatrix} \tag{2.9}$$

Finding θ

To find θ, the algorithm will first find the triplet between which the rotor's electrode has the most facing area and use the value of the 3 capacitances inside this triplet. The matrix of those 3 capacitances will be named C_θ :

$$C_\theta = max\left(\begin{pmatrix} C_1 \\ C_2 \\ C_3 \end{pmatrix}, \begin{pmatrix} C_{3n-2} \\ C_{3n-1} \\ C_{3n} \end{pmatrix}, ..., \begin{pmatrix} C_{3N-2} \\ C_{3N-1} \\ C_{3N} \end{pmatrix}\right) \tag{2.10}$$

The 3 values of the capacitances inside a triplet always follow the same pattern (in this example, the matrix C_θ is composed of the 3 capacitances of the 1^{st} triplet):

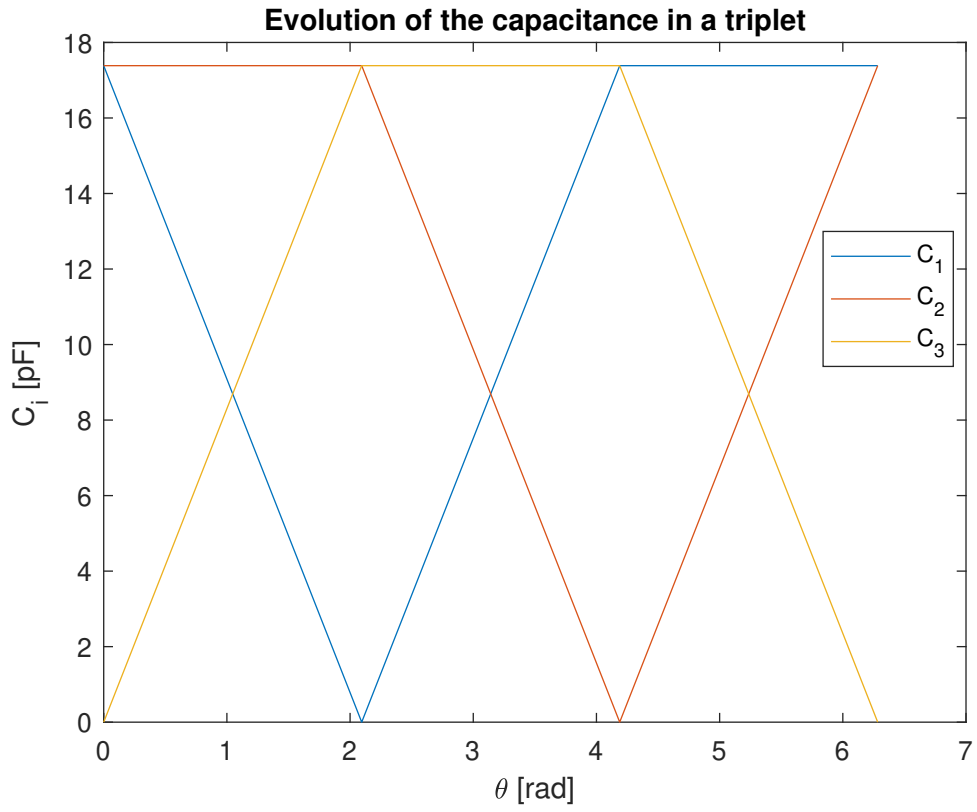

Figure 2.6: Evolution of the capacitances inside a triplet for a complete rotation with a fixed axial position

The algorithm will then work as follows :
The highest value between $C_{\theta,1}, C_{\theta,2}$ and $C_{\theta,3}$ will give the interval in which θ is located :

$$if\ max(C_{\theta,1}, C_{\theta,2}, C_{\theta,3}) == C_{\theta,2} : \theta \in [0, \frac{2\pi}{3}] \tag{2.11}$$

$$if\ max(C_{\theta,1}, C_{\theta,2}, C_{\theta,3}) == C_{\theta,3} : \theta \in [\frac{2\pi}{3}, \frac{4\pi}{3}] \tag{2.12}$$

$$if\ max(C_{\theta,1}, C_{\theta,2}, C_{\theta,3}) == C_{\theta,1} : \theta \in [\frac{4\pi}{3}, 2\pi] \tag{2.13}$$

Then the fraction of one of the 2 other values over the largest will situate θ in the given interval :

$$if\ max(C_{\theta,1}, C_{\theta,2}, C_{\theta,3}) == C_{\theta,2} : \theta = 0 + \frac{C_{\theta,3}}{C_{\theta,2}} \frac{2\pi}{3} \tag{2.14}$$

$$if\ max(C_{\theta,1}, C_{\theta,2}, C_{\theta,3}) == C_{\theta,3} : \theta = \frac{2\pi}{3} + \frac{C_{\theta,1}}{C_{\theta,3}} \frac{2\pi}{3} \tag{2.15}$$

$$if\ max(C_{\theta,1}, C_{\theta,2}, C_{\theta,3}) == C_{\theta,1} : \theta = \frac{4\pi}{3} + \frac{C_{\theta,2}}{C_{\theta,1}} \frac{2\pi}{3} \tag{2.16}$$

Finding z

To find the z position, the algorithm will use the matrix C_z that is a 1xN matrix containing the sum of the 3 capacitances inside each triplet :

$$C_z = \left(sum \begin{pmatrix} C_1 \\ C_2 \\ C_3 \end{pmatrix}, sum \begin{pmatrix} C_{3n-2} \\ C_{3n-1} \\ C_{3n} \end{pmatrix}, ..., sum \begin{pmatrix} C_{3N-2} \\ C_{3N-1} \\ C_{3N} \end{pmatrix} \right) \tag{2.17}$$

Those sums follow the pattern shown on the following figure (in this example, N=3):

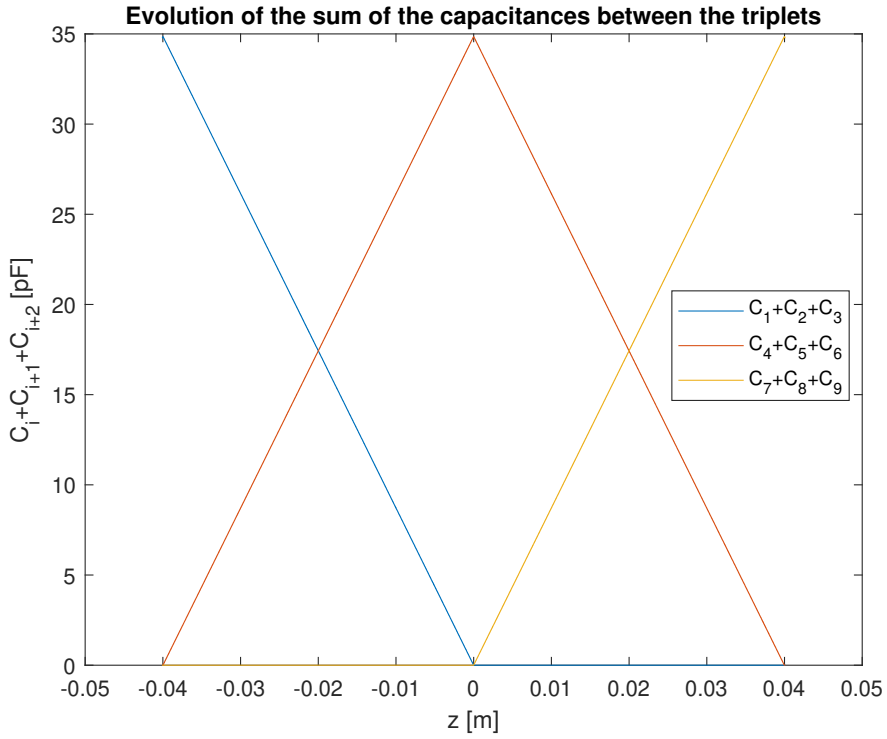

Figure 2.7: Evolution of the sum of the capacitances between the triplets for a displacement of length Δ_z in the axial direction with a fixed axial position

In the C_z matrix, two values are not equal to zero, they will be called $C_{z,i}$ and $C_{z,j}$. Those 2 non-zeros values will give the interval in which z is located and again the characteristic being linear the ratio $\frac{C_{z,i}}{C_{z,i}+C_{z,j}}$ or $\frac{C_{z,j}}{C_{z,i}+C_{z,j}}$ will situate z in the given interval.

2.3 In-depth analysis

Until now, the model has been studied considering an ideal case where no parasitic capacitances are taken into account and where all the electrodes are next to each other. This section will therefore study the influence of the different parameters on the ability to retrieve the position.

2.3.1 d_z parameter

The first parameter that will be studied is d_z, the axial distance between 2 outer electrodes.

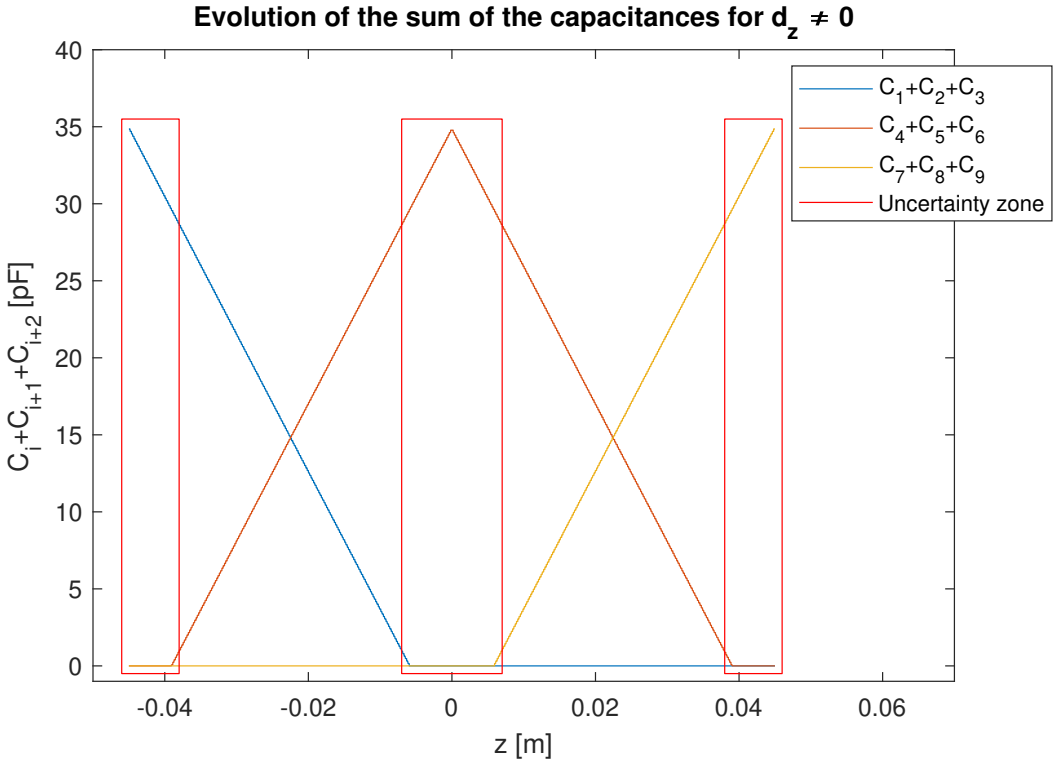

Figure 2.8: $d_z = 6mm$

As illustrated on figure 2.8, having $d_z \neq 0$ will lead to the appearance of different zone of uncertainty in which only one value is different from zero. It is then impossible to situate z with precision in this interval. This uncertainty on the position happens in fact when the rotor is only facing one triplet of electrodes and will remain until it faces 2 triplets again. This phenomenon is illustrated on figure 2.9

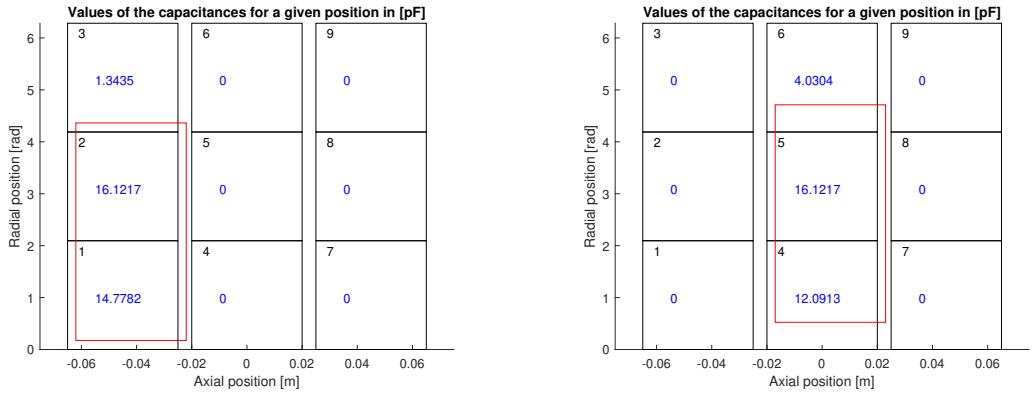

(a) $\theta = 10$ [°], $z = -0.042$ $[m]$ (b) $\theta = 30$ [°], $z = 0.003$ $[m]$

Figure 2.9: Rotor's electrode positions leading to uncertainty

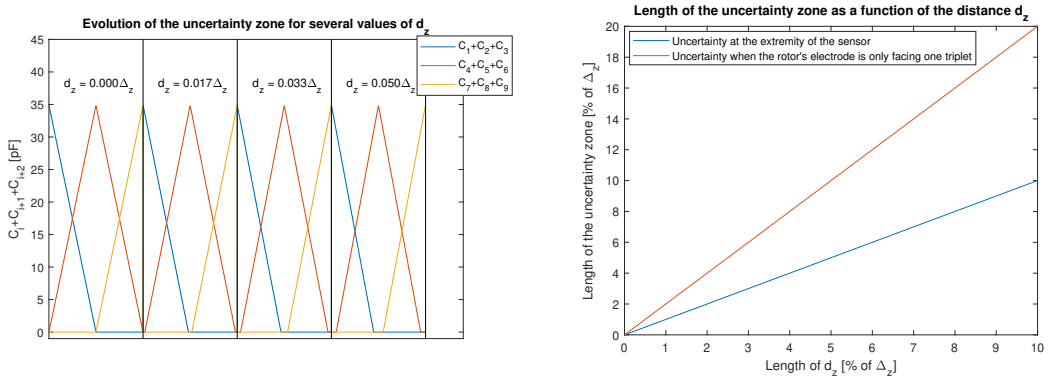

Figure 2.10: Evolution of the uncertainty zone as a function of d_z

This uncertainty will increase as d_z increases. According to figure 2.10, the range of this uncertainty zone will increase linearly and will be equal to $2d_z$. It is easy to imagine that the number of uncertainty zones will increase as N increases too. It is therefore important to minimize the gap d_z in order to limit those uncertainty zones and to choose a number of triplet N that is as small as possible.

2.3.2 d_θ parameter

In this section, the impact of the parameter d_θ on the measuring range will be studied

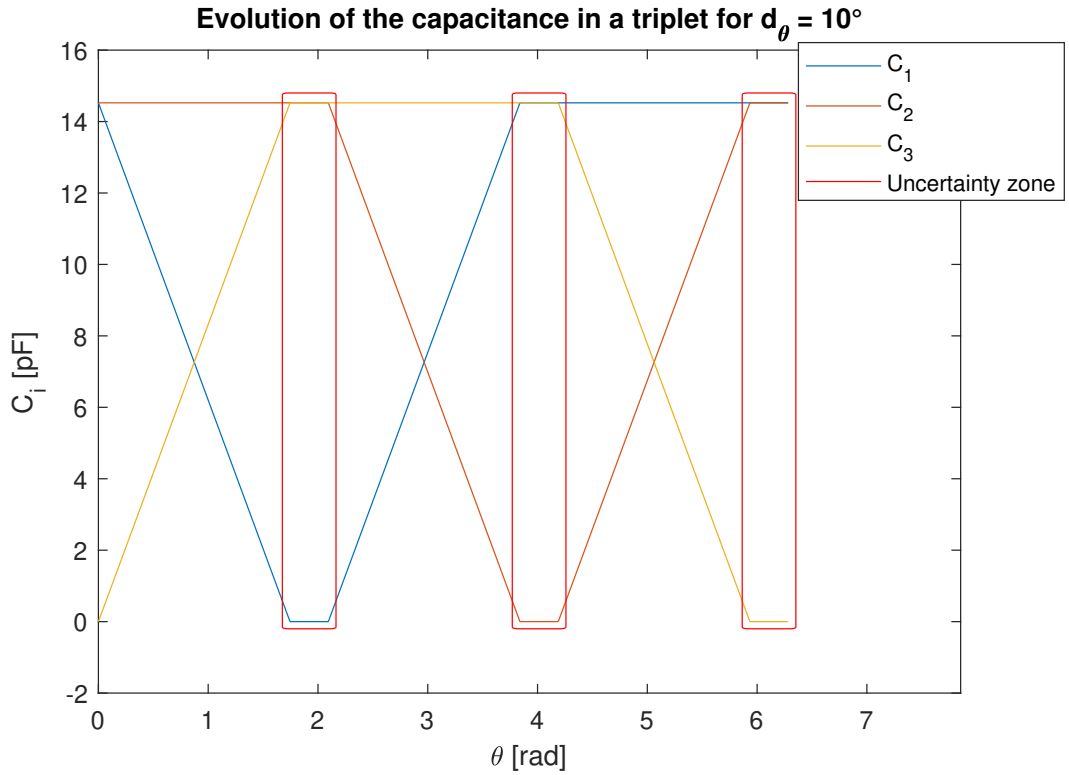

Figure 2.11: Evolution of the capacitances in a triplet for a= angle $d_\theta \neq 0$

As for d_z, the consequence of an angle d_θ different from zero will lead to the appearance of uncertainty zones where the algorithm won't be able to locate the angle θ with precision. Those uncertainty zones appear, as depicted on figure 2.12, when the inner electrode is only facing 2 of the 3 outer electrodes of a triplet.

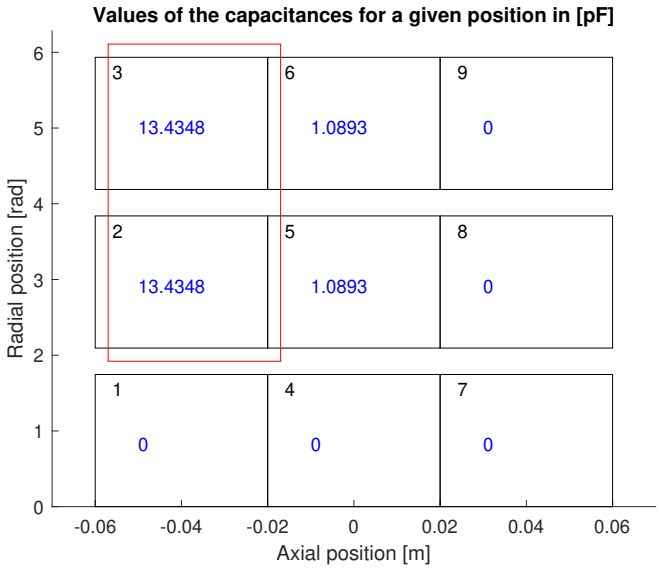

Figure 2.12: $d_\theta = 20$ [°], $z = -0.037$ $[m]\theta = 110$ [°]

As illustrated on figure 2.13, the length on the uncertainty zone will increase linearly as the angle d_θ increases. The length of this uncertainty zone will be equal to the angle d_θ and it is also important to notice that the maximum value of the characteristic will decrease as d_θ increases. In the considered ideal case, this won't have any consequences on the measuring precision but in a case where noises and parasitic capacitances are taken into account, they will become more important in front of this maximum value. In order to ensure a measure as accurate as possible, the prototype will thus be designed in a way to have d_θ as small as possible.

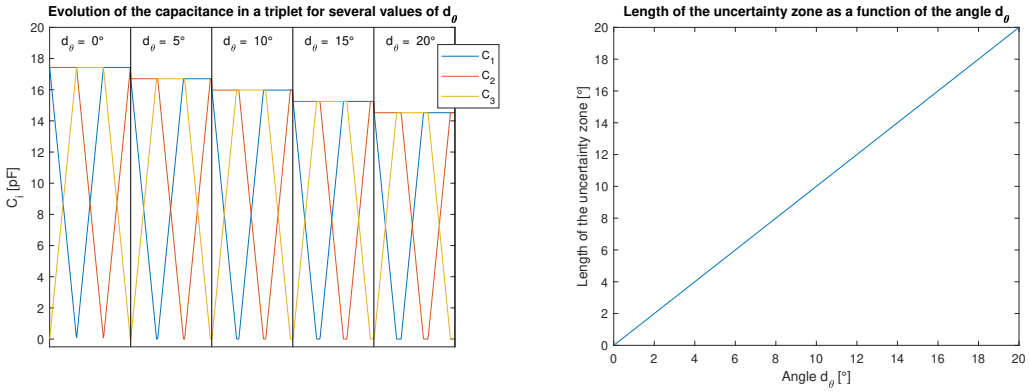

Figure 2.13: Evolution of the uncertainty zone as a function of d_θ

2.3.3 d parameter

The last parameter that will be studied is d, the radius difference between the inner and outer electrode. As illustrated on figure 2.14 and 2.15, the increase of the distance d will lead to a logarithmic decrease of the maximum possible values of the measured capacitances. This is simply due to the denominator term of the capacitance formula $\ln(\frac{R_b}{R_a})$ as $d = R_b - R_a$. Again, this will lead to accuracy diminutation as the noises and parasitic capacitances will become more important in front of the measured values. The sensor will therefore be designed in a way to have the smallest possible distance between the electrodes.

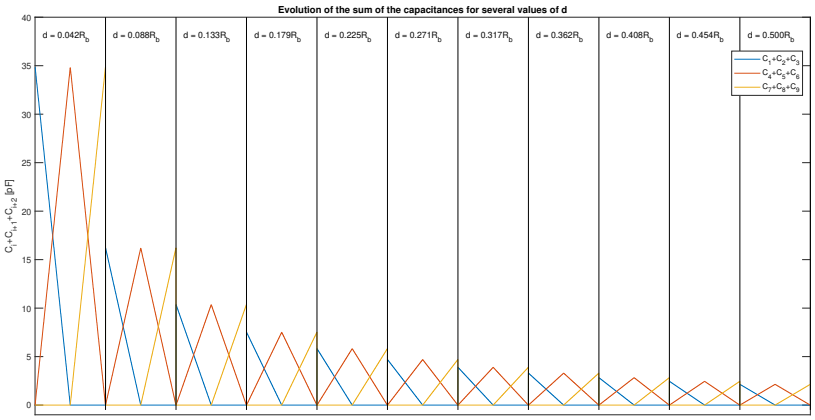

Figure 2.14: Evolution of the sum of the capacitances between the triplets as a function of d

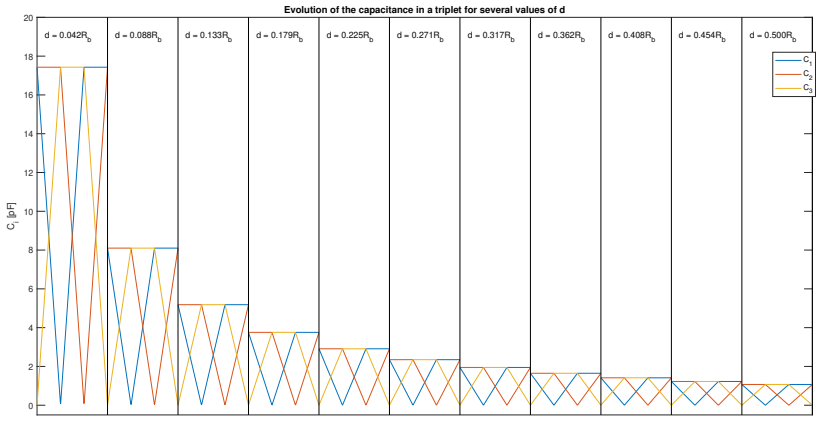

Figure 2.15: Evolution of capacitances inside a triplet as a function of d

2.3.4 Influence of the parasitic capacitances

Until now, the measurement analysis have been done in an ideal world where no noises and parasitic capacitances are taken into account. This is of course not the case, this section will therefore study the behaviour of the previous results by considering those non idealities.

Parasitic capacitances inside a triplet

Firstly, only the parasitic capacitances inside a triplet will be considered, so without taking into account the adjacent triplets. The modification made compared to the ideal case is the consideration of a parasitic capacitance C_{par} due to the coplanarity of 2 nearby outer electrodes. Both cases, when the inner electrode is facing the triplet or not, will be considered. The addition of the parasitic capacitance when the inner electrode is facing the triplet is shown on figure 2.16 with the corresponding equivalent circuit.

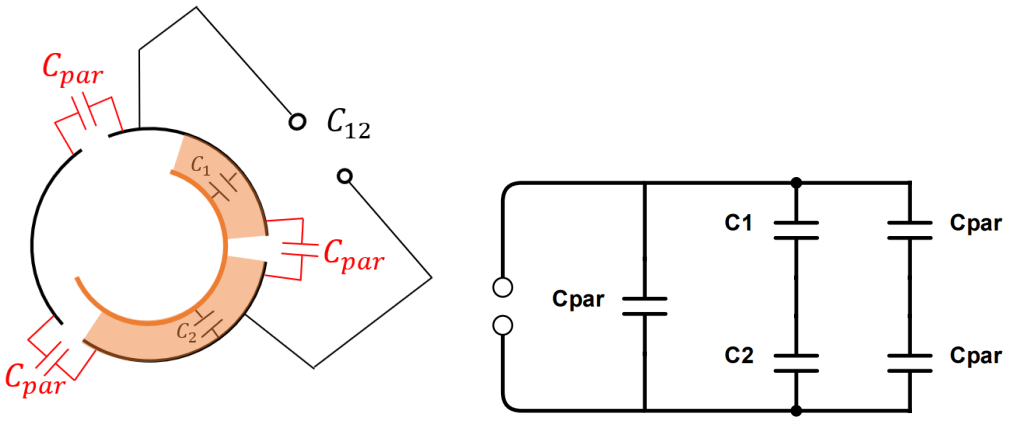

(a) Capacitances measured between two outer electrodes

(b) Equivalent circuit

Figure 2.16: Parasitic capacitances when measuring between 2 outer electrodes when the inner electrode is facing the triplet.

By using the formulas of capacitances in series and in parallel, the following result is obtained :

$$C_{i,j} = C_{par} + (\frac{1}{C_i} + \frac{1}{C_j})^{-1} + (\frac{1}{C_{par}} + \frac{1}{C_{par}})^{-1} = (\frac{1}{C_i} + \frac{1}{C_j})^{-1} + \frac{3}{2}C_{par} \quad (2.18)$$

The real measured capacitance between two outer electrodes will then remain the same as in the basic case with the different that a constant term equal to $\frac{3}{2}C_{par}$ has been added. When measuring the capacitance between 2 outer electrodes, if the inner electrode is not facing the triplet, the following configuration will be obtained :

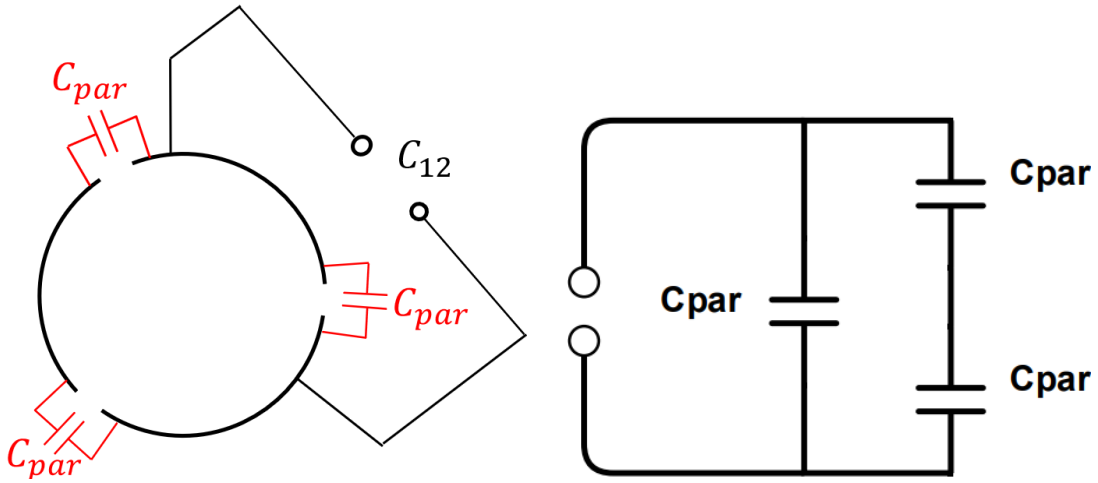

(a) Capacitances measured between two outer electrodes

(b) Equivalent circuit

Figure 2.17: Parasitic capacitances when measuring between 2 outer electrodes when the inner electrode is not facing the triplet.

As calculated in equation 2.19, the measured capacitance will not be equal to zero anymore but to a constant value equal to $\frac{3}{2}C_{par}$.

$$C_{i,j} = C_{par} + (\frac{1}{C_{par}} + \frac{1}{C_{par}})^{-1} = \frac{3}{2}C_{par} \tag{2.19}$$

Approximation of C_{par}

The value of C_{par} will be approximate using equation 2.20. This is the equation of the capacitance made between 2 coplanar electrodes of width w, length l and with a separation distance s (figure 2.18).

$$C_{par} = \frac{\epsilon_r l_b \ln\left(-\frac{2}{\sqrt[4]{1-\frac{s^2}{(s+2w)^2}}-1}\left(\sqrt[4]{1-\frac{s^2}{(s+2w)^2}}+1\right)\right)}{377\pi v_0} \tag{2.20}$$

With :

- ϵ_r : The relative permittivity of the dielectric between the electrodes. As the dieletric used in the model is air, $\epsilon_r = 1$.
- v_0 : The speed of light in a vacuum : 2997948 [m/s].
- s : The separation between the electrodes.

- w : The width of the electrodes.

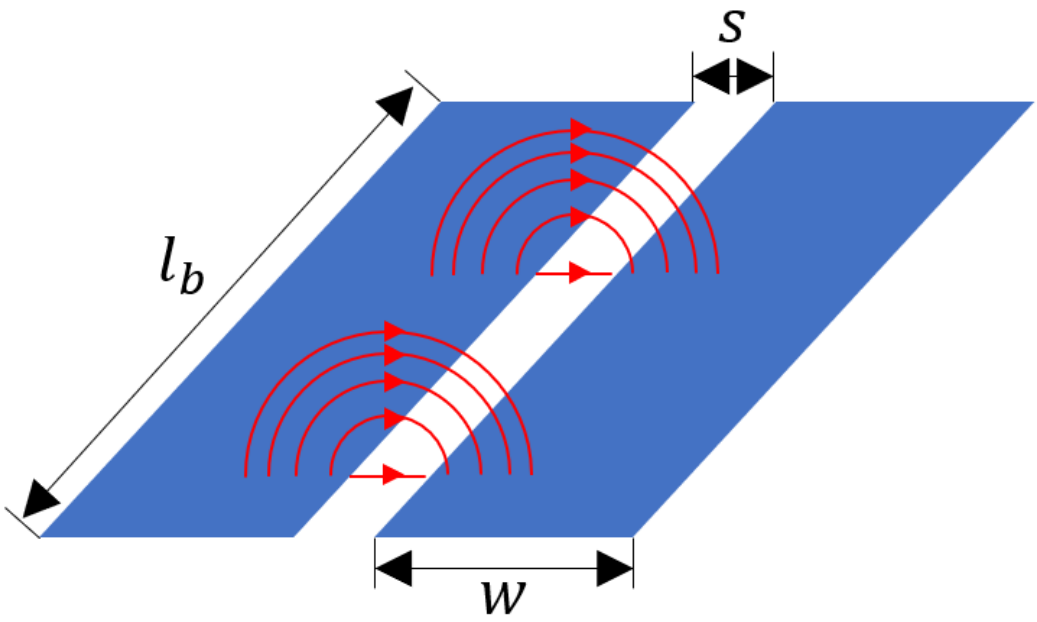

Figure 2.18: Coplanar electrodes notations

As the 2 electrodes are not perfect planes but cylindrical, the following assumptions have been done :

- The separation s between the electrodes will be approximated by $R_b d_\theta$.
- The outer electrodes have an angle of revolution of $\frac{2\pi}{3}$ but as they are not perfect planes, the width w will be approximated by $\frac{\pi}{3} R_b$. Which means that the 2 electrodes are considered as coplanar planes of a width equal to the half of their angle of revolution.

To validate this last approximation, the graph of this parasitic capacitance in function of the length of the electrode w has been plotted on figure 2.19.

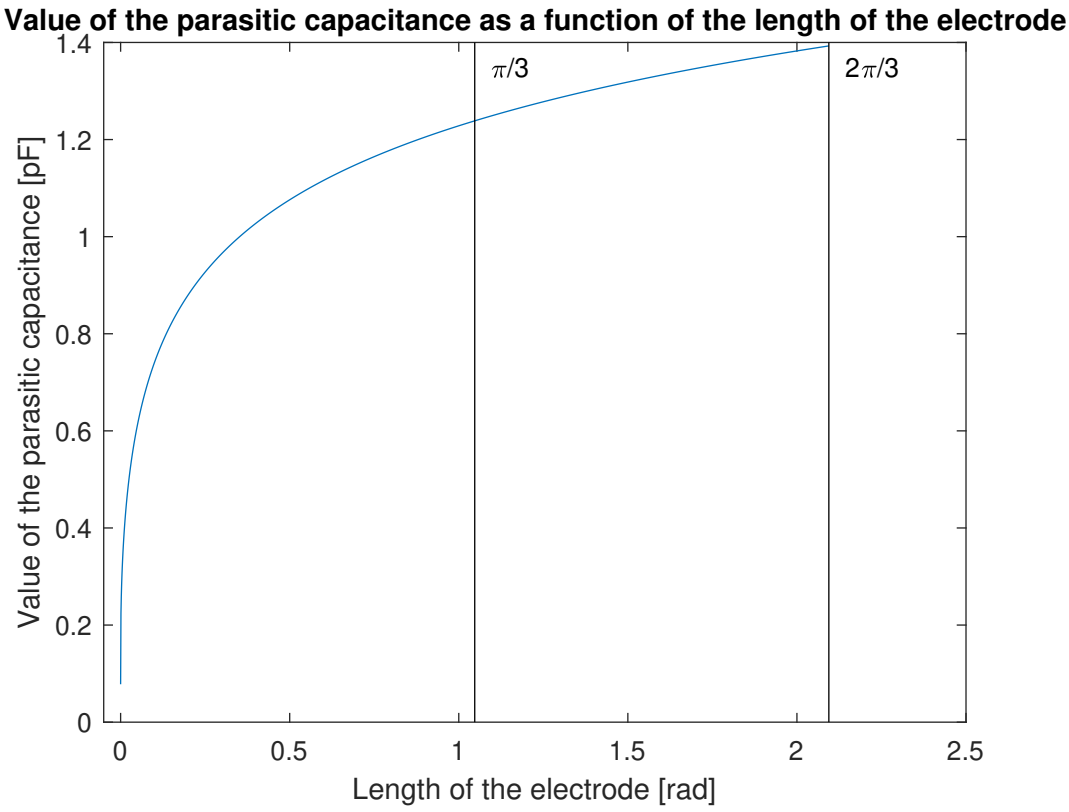

Figure 2.19: Value of the parasitic capacitance in function of its length for $d_\theta = 0.5\ [°], l_b = 4\ [cm]$ and $R_b = 12\ [mm]$

As illustrated, the length of the electrodes will mainly have an impact in the first half of his length having a difference of less than 14 % between an electrode of length $\frac{\pi}{3}R_b$ and $\frac{2\pi}{3}R_b$. This approximation is therefore acceptable.

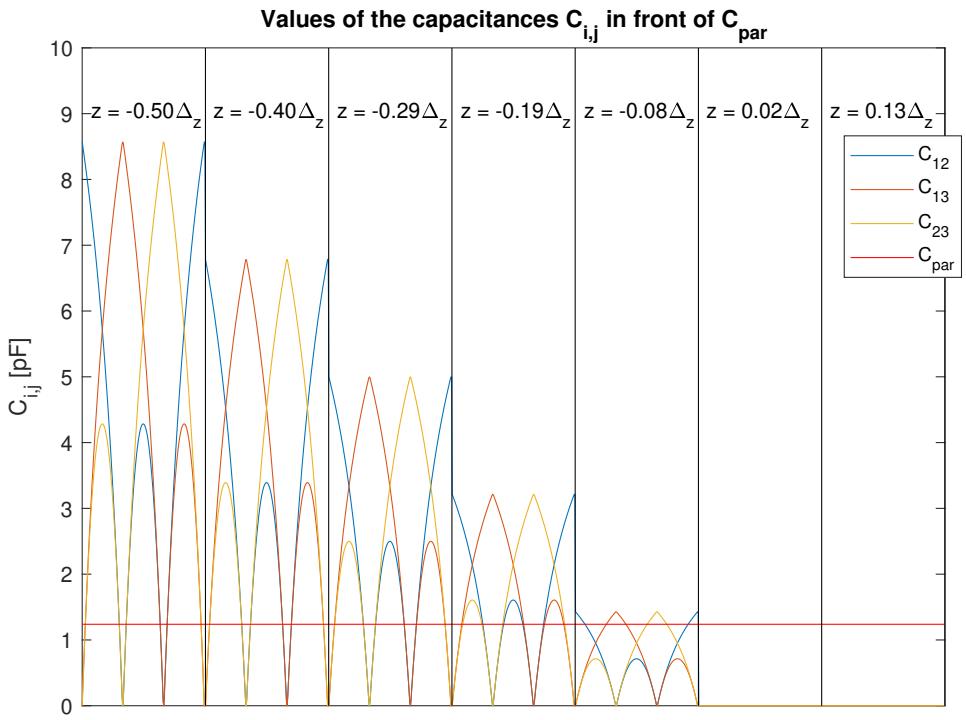

Figure 2.20: $d_\theta = 1$ [°], $N = 3, R_a = 11.5$ [mm] and $R_b = 12$ [mm]

The value of the capacitance C_{par} in front of the measured capacitances $C_{i,j}$ for several z positions is shown on figure 2.20. As it is a constant value, taking this parasitic capacitance into account can simply be handled by the algorithm by removing it before the computation of the position.

Complete approach

To be complete, additionnal parasitic capacitances should be added to the previous model. Indeed, as illustrated on figure 2.21, capacitances from the adjacent triplets have to be taken into account to evaluate the real measured capacitance between 2 outer electrodes.

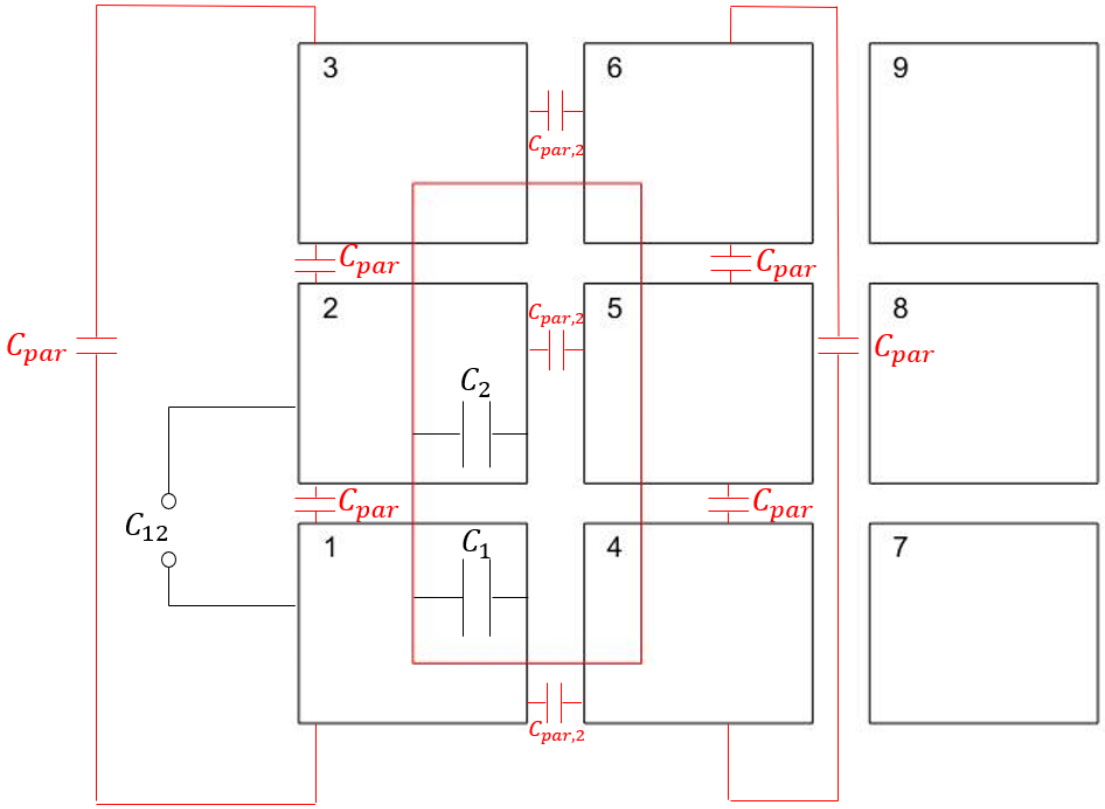

Figure 2.21: Full model of the parasitic capacitances

As the new model becomes complex and may not consider all the pertubations and parasitic capacitances, it has been decided not to study it in an analytical way. An approach using the finite element method that will simulate in a more precise way the interactions between the electrodes will therefore be taken. This approach will be described in the next chapter.

2.3.5 e_a,e_b parameter

As the parameters e_a and e_b do not intervene in the formula of the capacitance, the only impact that the thickness of an electrode could have is the apparition of a new parasitic capacitance in the model. As nowadays manufacturing processes allow to have PCBs with copper layers up to 18 $[\mu m]$, the influence of this parameter has been neglected.

Chapter 3

Sensor FEM modelling

This chapter will study the behaviour of the sensor using the finite element method through the computer software Comsol. Comsol is a complete finite element software capable of simulating different phenomena of the everyday life as fluid flows, heat transfers, structural mechanics or even, in this case, electromagnetics interactions.

3.1 Model description

The model has been realised based on parametrical values in order to be able to change them without having to recreate a model when simulating other parameters. The only simplification that has been done is considering the electrodes as surfaces instead of volumes in order to reduce the simulation time. Again, as nowadays manufacturing processes allow to have copper surfaces with a thickness up to 18 $[\mu m]$ in PCBs, this is a reasonable approximation. In order to consider all the parasitic capacitances, when simulating the capacitance between 2 outer electrodes, all the other surfaces have been set to "floating potential" surfaces.

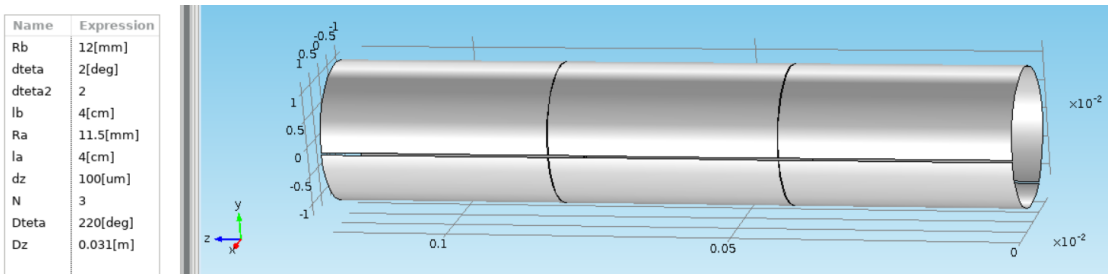

Figure 3.1: Comsol model

As justified in the previous section, as the parameters d, d_θ, d_z have to be as small

as possible and in order to have a range of working of 8 [cm] and 360 [°], the simulations have been done with the following specifications :

- $d_\theta = 2$ [°]
- $d_z = 0.1$ $[mm]$
- $l_b = l_a = 4$ $[cm]$
- $N = 3$
- $R_b = 12$ $[mm]$
- $R_a = 11.5$ $[mm]$

d_θ and d_z have been fixed according to the typical track-to-track distance attainable in PCBs and R_a and R_b according to the motor prototype size described in the introduction. Then, in order to have a compromise between simulation time and result sample size, each capacitances $C_{i,j}$ have been computed under a parametric sweep in the range $[-0.04, 0.04]$ $[m]$ and $[0, 360]$ [°] with a step of 5 [°] and 1 [mm]. This means that 5832 positions have been computed for each capacitance $C_{i,j}$.

3.2 Results

The 2 graphs shown on figure 3.2 represent the computed values of $C_{i,j}$ for all the considered positions where the 360 [°] revolutions for each z position have been placed next to each other.

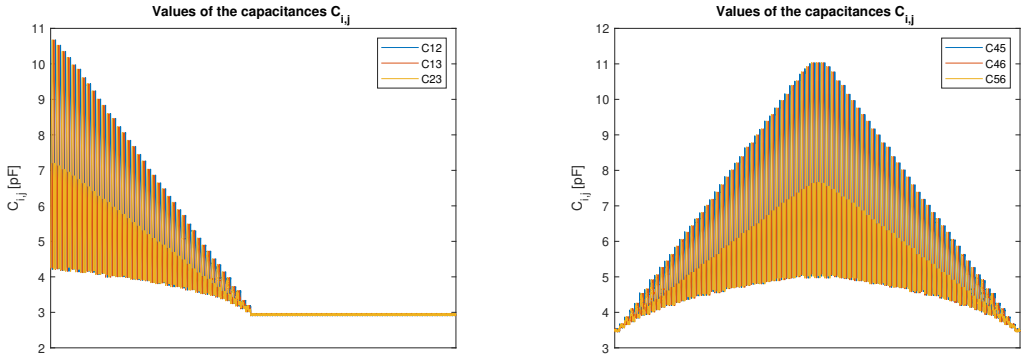

(a) Capacitances $C_{i,j}$ in the first triplet (b) Capacitances $C_{i,j}$ in the second triplet

Figure 3.2: Computed values of $C_{i,j}$ for the total z displacement

Those graphs show that as highlighted in the previous section, a constant parasitic value is observed when the rotor's electrode is not facing the triplet but the main difference is that this parasitic capacitance will not be constant and increase as the inner electrode gets close to the concerned triplet. However, the different capacitances C_i have been computed on the basis of the computed capacitances $C_{i,j}$ to evaluate the impact of this offset on the measurability of the sensor.

3.2.1 Impact on the z measurability

As observed on figure 3.3, the 2 sums of the extremity triplet undergo an offset of approximately 18 $[pF]$ but the sum of the triplet of the middle has an offset slightly higher than the 2 others. However, as the characteristic remains linear, the z position could easily be retrieved by removing those non-idealities through a calibration of the sensor to measure the 2 different offsets.

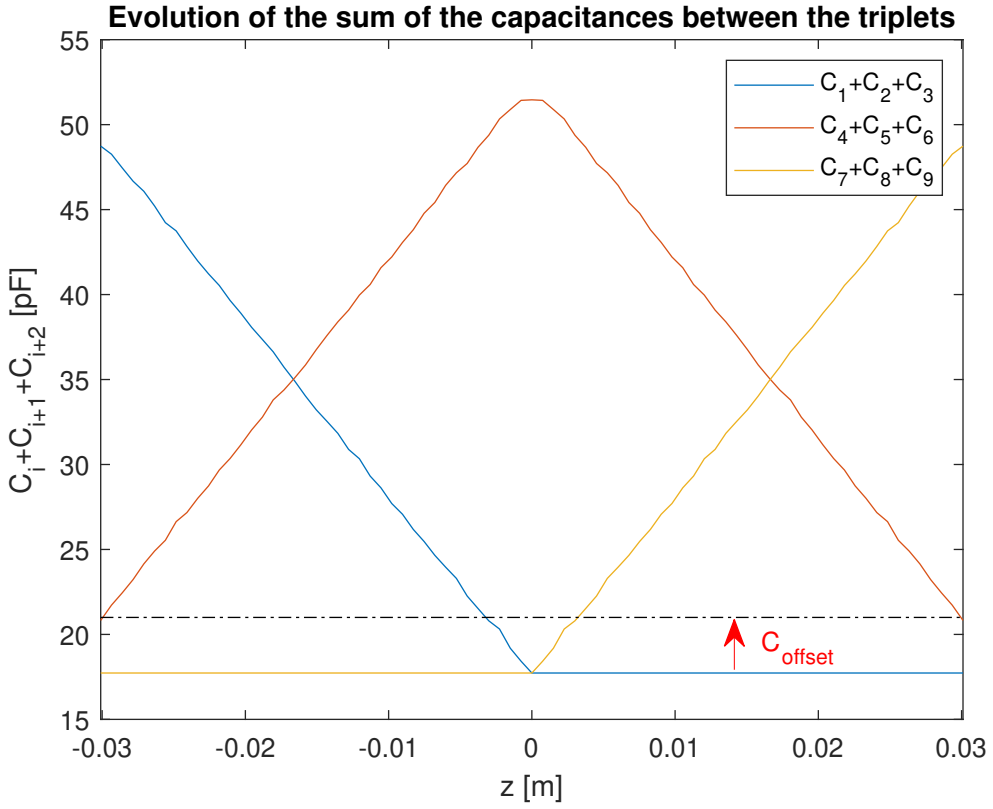

Figure 3.3: Evolution of the sum of the capacitances between the triplets

3.2.2 Impact on the θ measurability

The graph of the evolution of the capacitances inside a triplet is shown on figure 3.4. As for the sums of capacitances, an offset is observed and the characteristic remains linear in a large part of the characteristic but the issue is the appearance of peaks around $0°, 120°, 240°$ and $360°$. As explained in chapter 2, the algorithm uses the highest value to find the interval in which θ is located. Those peaks will therefore lead to trouble retrieving the position as the highest value is often inverted with the expected value.

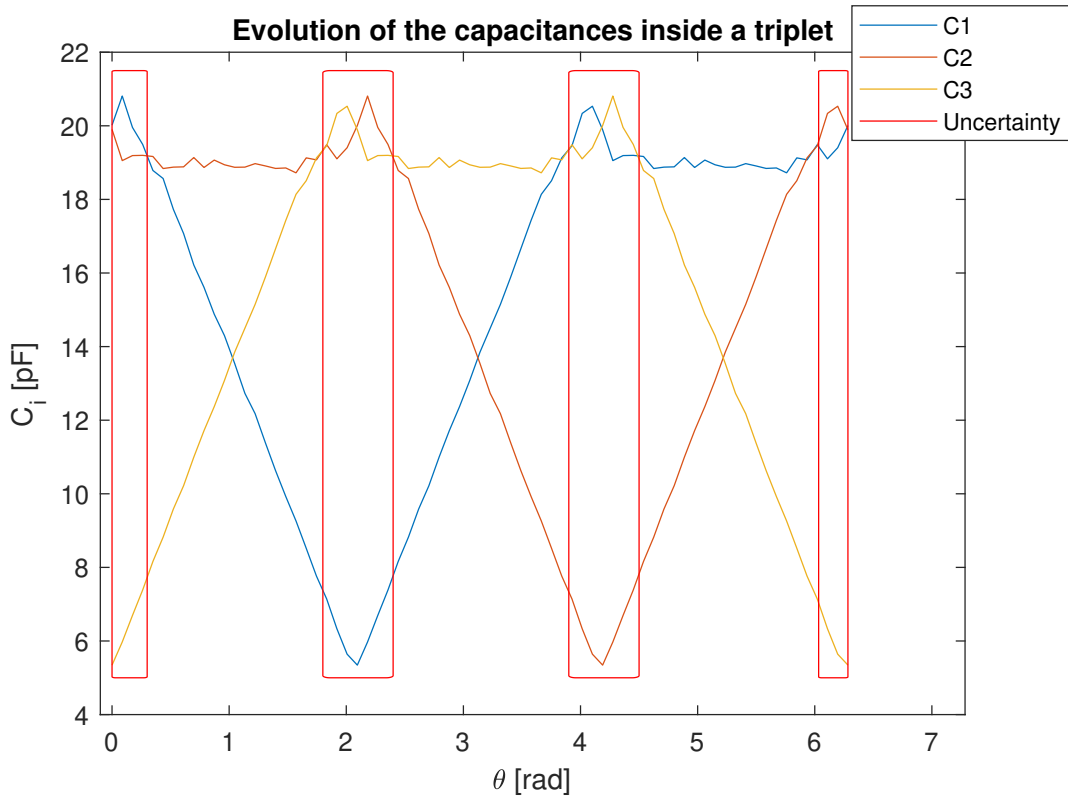

Figure 3.4: Evolution of the capacitances inside a triplet

The use of finite element has mostly confirmed the results obtained in the previous chapter but the differences will have to be taken into account in the algorithm in order to retrieve the position with the highest precision possible.

Chapter 4

Positioning algorithm

As highlighted in the previous chapter, the use of finite element have brought modifications to the expected analytically computed values. This chapter will therefore propose different algorithm that have been developped in order to retrieve the position. Each algorithm has been tested using as input the computed values by the finite element software and their precision have been compared.

4.1 Reviewed initial algorithm

The first algorithm that has been tested is an upgraded version of the initial algorithm that takes into account the non-idealities. As for the basic version, the first step will be to compute the capacitances C_i from the capacitances $C_{i,j}$:

$$f(\begin{pmatrix} C_{1,2} & C_{3n-2,3n-1} & ... & C_{3N-2,3N-1} \\ C_{1,3} & C_{3n-2,3n} & ... & C_{3N-2,3N} \\ C_{2,3} & C_{3n-1,3n} & ... & C_{3N-1,3N} \end{pmatrix}) = \begin{pmatrix} C_1 & C_{3n-2} & ... & C_{3N-2} \\ C_2 & C_{3n-1} & ... & C_{3N-1} \\ C_3 & C_{3n} & ... & C_{3N} \end{pmatrix} \tag{4.1}$$

4.1.1 Retrieve the z position

As shown on figure 5.8, to retrieve the z position, the offsets will be removed in order to bring both curves between the same range of values but also to bring them as close as possible to zero. The z position will then be computed using the method explained in chapter 2.

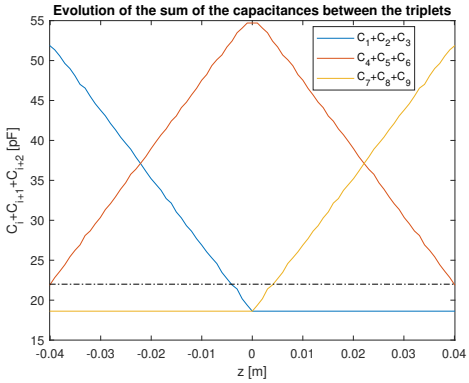

(a) Sum of the capacitances before modification

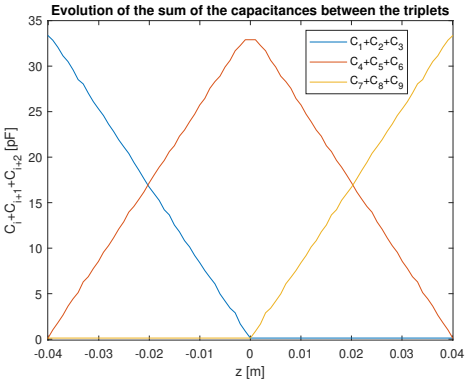

(b) Sum of the capacitances after modification

Figure 4.1: Modifications brought to the characteristics

4.1.2 Retrieve the θ position

To retrieve the θ position, 2 modifications have been brought to the characteristic :

- As for the z position, the offset has been removed in order to bring the curves as close as possible to zero.
- As the ratio between the highest value and 1 of the 2 others is used to compute the θ position, the 2 lines should intersect when they are equal to the half of the maximum value which is not the case. This is why a gain have been applied each time on the maximum value.

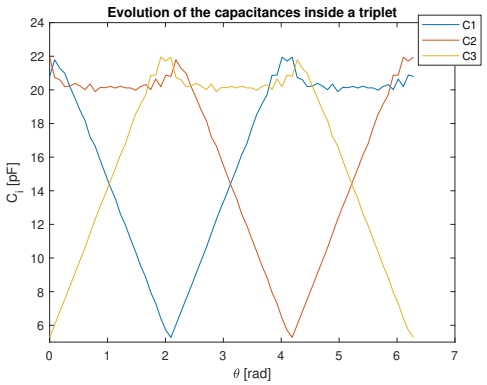

(a) Capacitances inside a triplet before modification

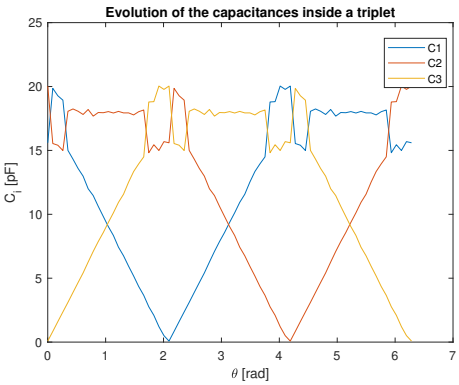

(b) Capacitances inside a triplet after modification

Figure 4.2: Modifications brought to the characteristics

4.1.3 Results

Using the capacitances computed by Comsol on this algorithm lead to the following results :

z precision					
Minimum error		Maximum error		Average error	
$1.37e^{-4}$ $[mm]$	$1.7e^{-4}$ [%]	0.9 $[mm]$	1.13 [%]	0.29 $[mm]$	0.36 [%]

θ precision					
Minimum error		Maximum error		Average error	
$1.1e^{-3}$ [°]	$3.1e^{-4}$ [%]	43.85 [°]	12.18 [%]	7.63 [°]	2.12 [%]

Concerning the z position, this algorithm scored a maximum error of 0.9 [mm] and an average error of 0.3 [mm] which represented 0.36 % of the total measuring range and is therefore under the desired precision. On the other hand, the obtained average error on the angle θ is 7.63 [°] with a maximal error up to 44 [°]. By looking on figure 4.3, those peaks of imprecision appear to come from the zones around 0,120,240 and 360 ° where the maximum value is inverted with the expected maximum value. Those results were expected but as the average error is close to 2 % for peaks up to 12 %, this means that the algorithm is doing well on the linear zones.

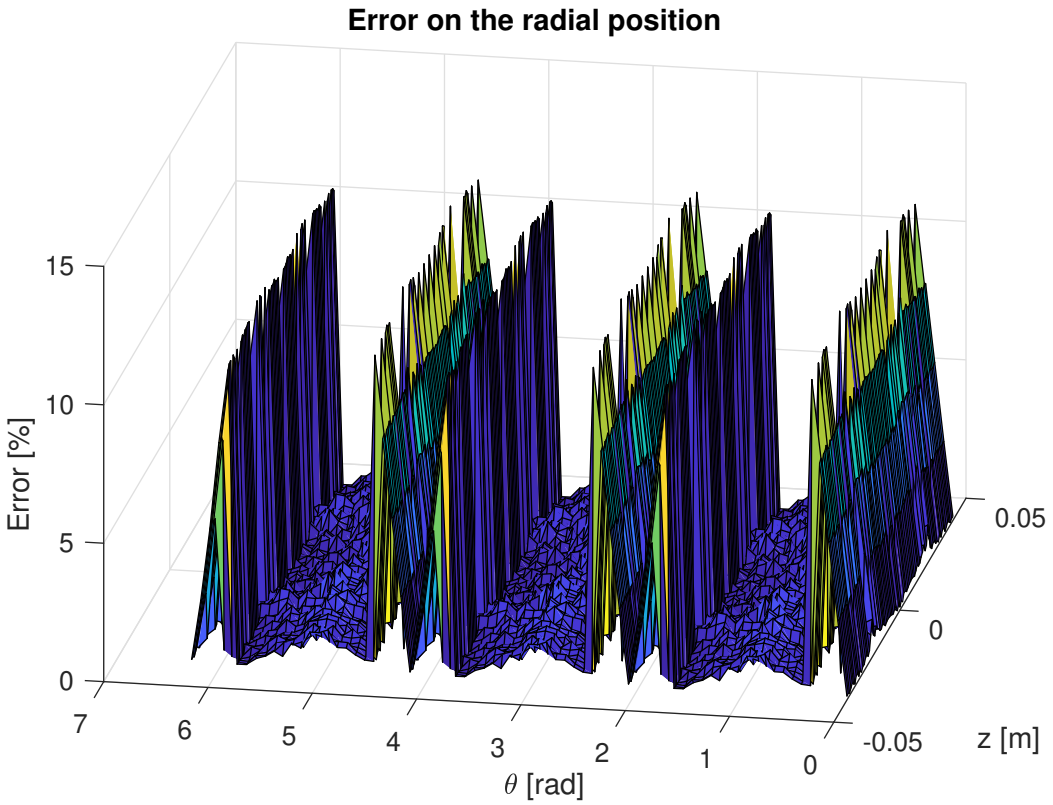

Figure 4.3: Error on the radial position using the first algorithm

4.2 Look-up table algorithm

This algorithm will be based on the working of look-up tables. More precisely, a reference table will be made regrouping a given number of matrix each corresponding to a given position (z, θ). Those matrixes being computed by means of a finite element reproduction of the sensor's model. The input matrix capacitance with the unknown position will then be compared with all the matrixes of the reference table. This will lead to a table of errors between the input matrix and the references matrixes. Then, the 2 positions corresponding to the 2 smallest errors will be used to compute a linear interpolation between the two positions in order to compute the final guessed position.

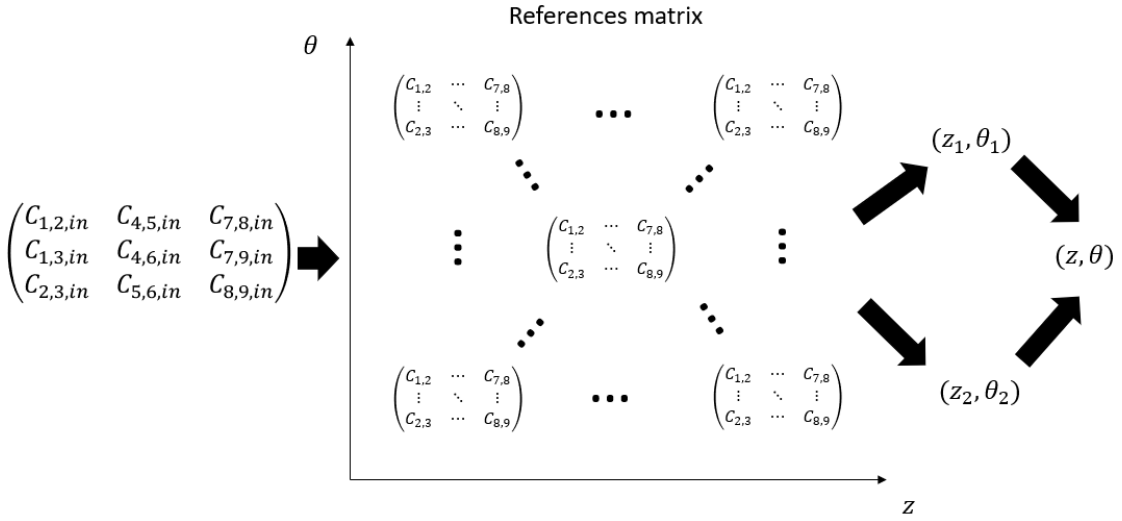

Figure 4.4: look-up table working

4.2.1 Results

For this algorithmn, the firstly computed capacitances have been used to build the look-up table : 5832 matrixes corresponding to z and θ positions within the range $[-0.04 : 0.001 : 0.04]$ $[m]$ and $[0 : 5 : 360]$ [°]. For the input matrixes, 4148 new positions have been computed in the range $[-0.0396 : 0.0012 : 0.0396]$ $[m]$ and $[0 : 6 : 360]$ [°].

Using this, the following results have been obtained :

z precision					
Minimum error		Maximum error		Average error	
3.17e^{-4} $[mm]$	3.9e^{-4} [%]	1.06 $[mm]$	1.32 [%]	0.18 $[mm]$	0.22 [%]

θ precision					
Minimum error		Maximum error		Average error	
0 [°]	0 [%]	38 [°]	10.55 [%]	4.17 [°]	1.16 [%]

Even if this algorithm is scoring almost 2 times better than the previous, the same phenomena is observed on figure 4.5 and errors on the radial position up to 38 [°] are obtained.

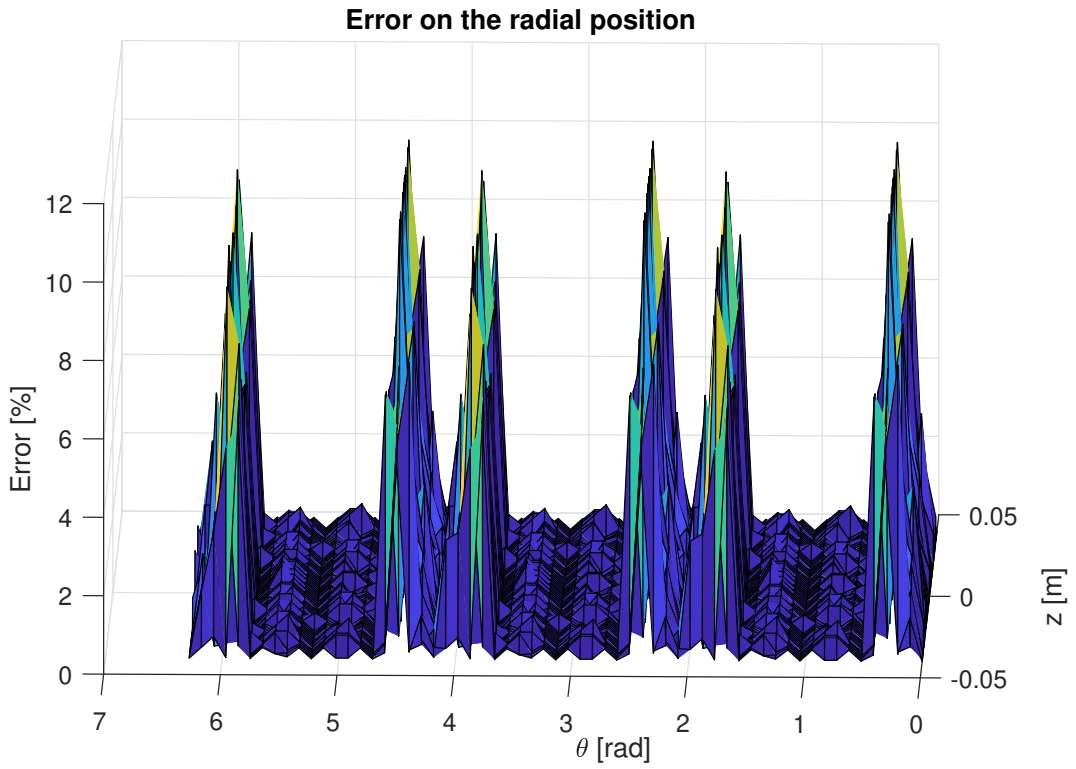

Figure 4.5: Error on the radial position for the second algorithm

4.3 Interpolation algorithm

This last algorithm is based on an interpolation process. As illustrated on figure 4.6, the graph of the capacitances $C_{i,j}$ for a fixed z position is composed of second degree polynomial curves and the 3 characteristics are the same to a shift of 120 [°].

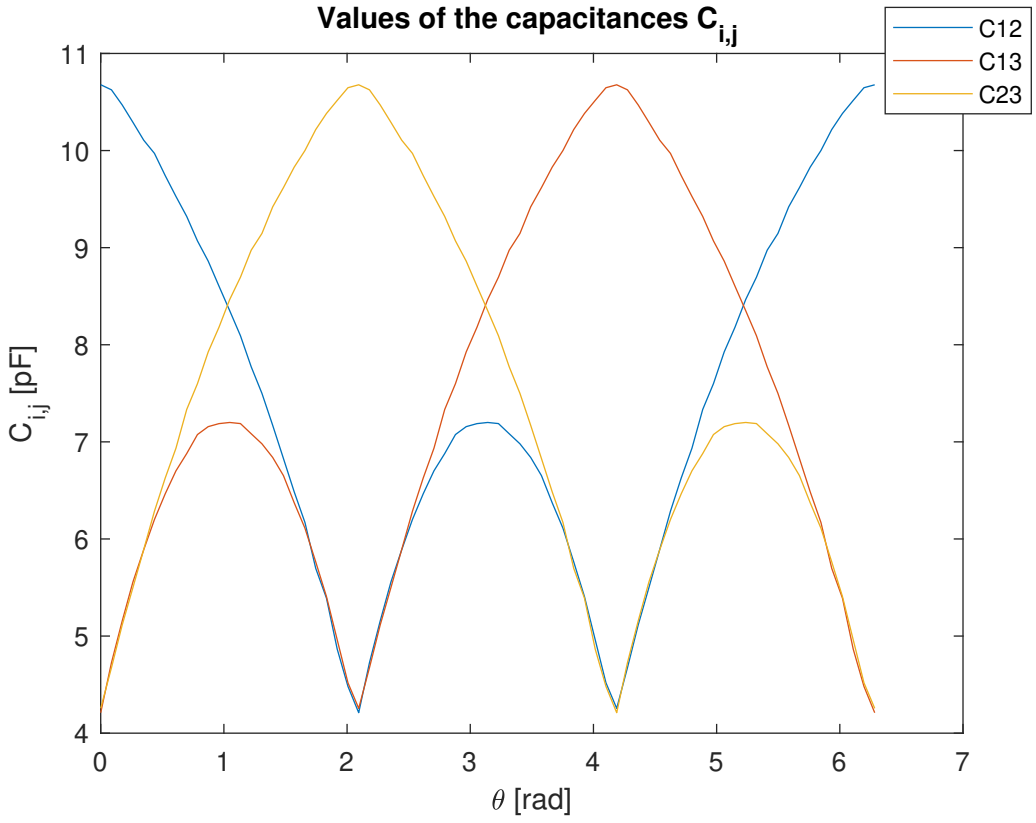

Figure 4.6: Values of the capacitances $C_{i,j}$ for a fixed z position

It is then possible to recreate this characteristic with very few known values. The graph on figure 4.7, for example, has been generated using only 4 known values of capacitances. It is then possible to retrieve the θ position by comparing the 3 input capacitances with this characteristic.

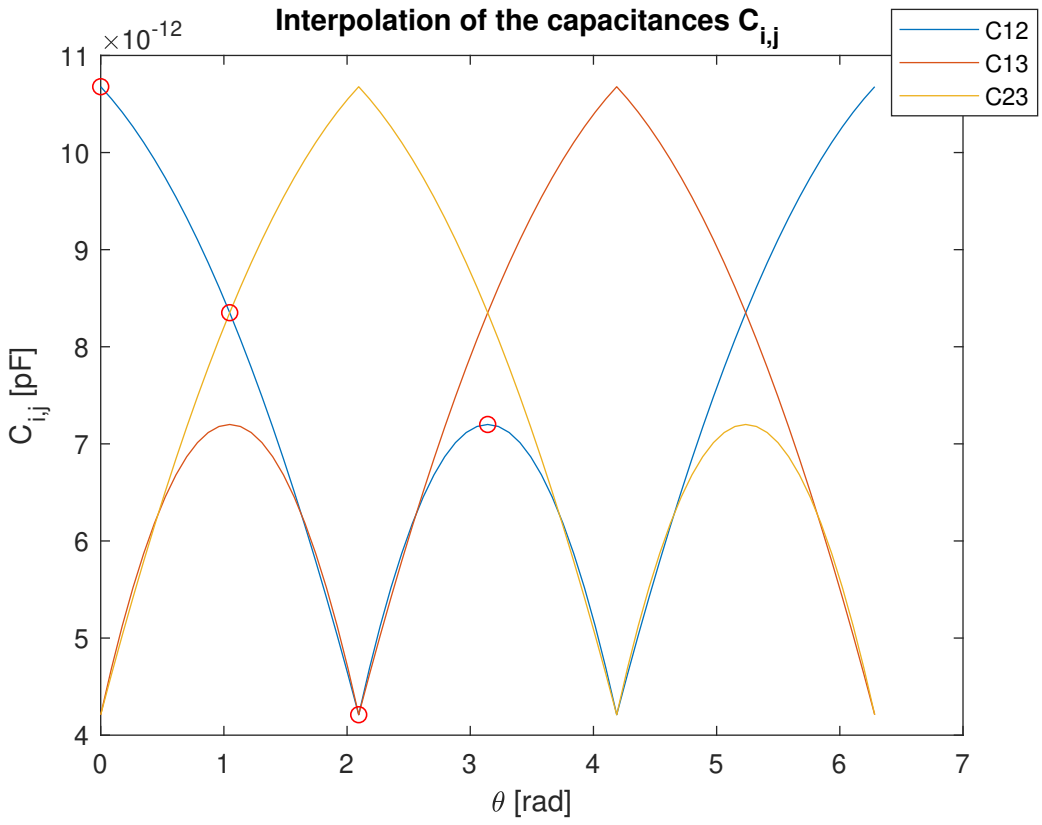

Figure 4.7: Interpolate characteristic with 4 points

Then in order to retrieve the angle for any z position, this would mean that 4 points are needed for each of them. However, as shown on figure 4.8, the maximum and minimum values between which this characteristic is defined are evolving linearly with the z position. This means that by knowing 4 points at a position z_1 and z_2, it is possible to recreate all the desired characteristics in the interval $[z_1; z_2]$.

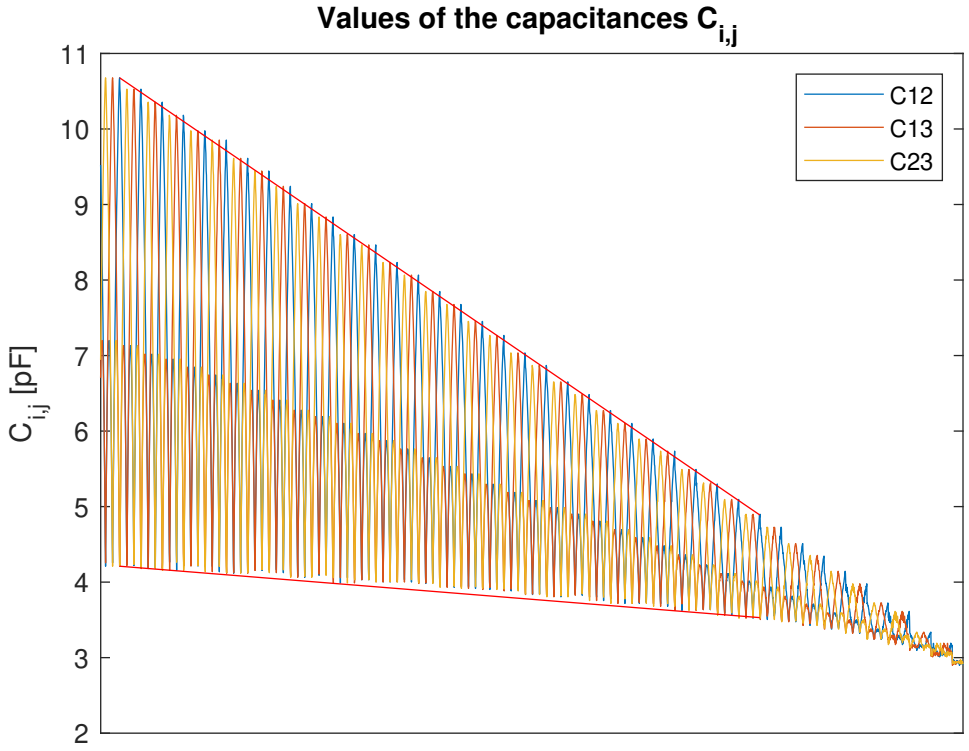

Figure 4.8: Shape of the characteristic in function of the z position

The algorithm works as follows :

- The z position is computed using the first proposed algorithm.
- The 4 needed values to recreate the characteristic are computed by interpolating linearly the 4 known values of z_1 and z_2.
- The 3 input capacitances are compared with the characteristic by resolving the corresponding second degree equations. This will lead to a list of potential angles.
- The potential angles are compared to keep the best solution.

4.3.1 Results

z precision					
Minimum error		Maximum error		Average error	
$1.37e^{-4}$ $[mm]$	$1.7e^{-4}$ [%]	0.9 $[mm]$	1.13 [%]	0.29 $[mm]$	0.36 [%]

θ precision					
Minimum error		Maximum error		Average error	
$1.9e^{-4}$ [°]	$6.8e^{-4}$ [%]	84.67 [°]	23.52 [%]	10.33 [°]	2.87 [%]

For the z position, as it uses the same method, the same precision is obtained. However this algorithm has the worst results when trying to compute the θ position with error peaks up to 85 [°]. As shown on figure 4.10, those errors again occur in the same zones, and this because 3 values of input capacitances are matching with 2 potential positions.

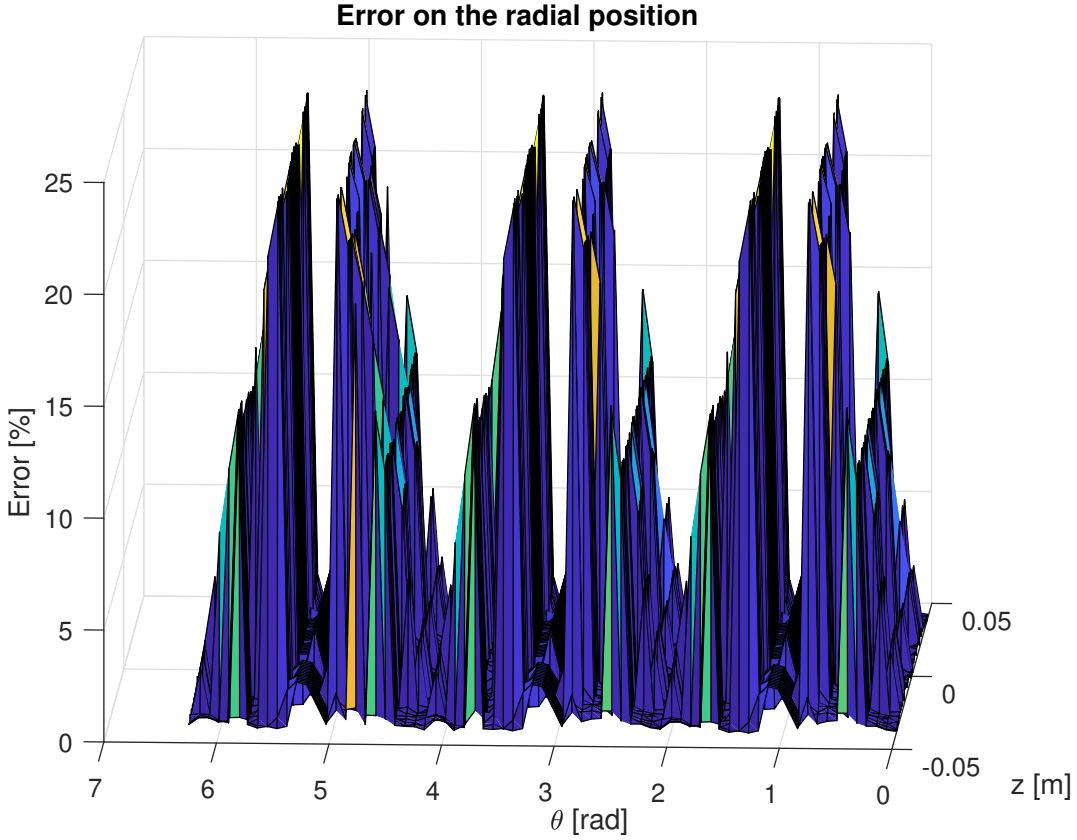

Figure 4.9: Error on the radial position for the second algorithm

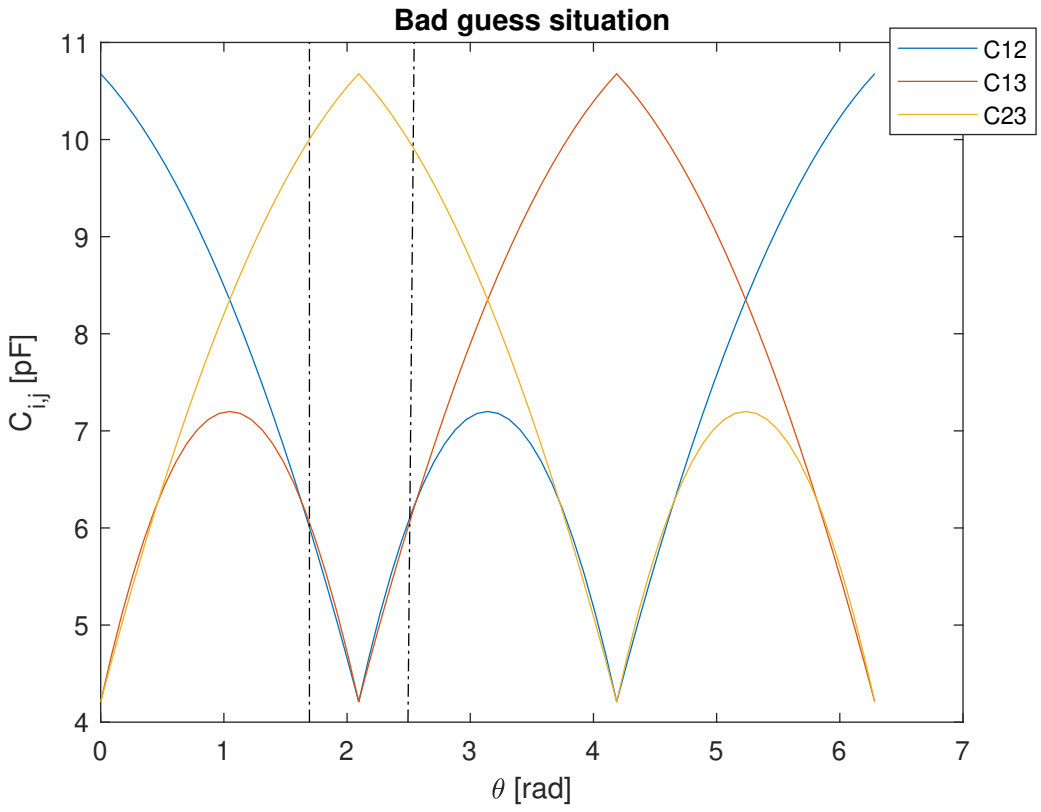

Figure 4.10: Bad guess situation

4.4 Proposed alternative

As the main cause of errors when trying to retrieve the θ position comes from the zones close to $0, 120, 240$ and 360 [°], different solutions have therefore been imagined to fix this issue. The following solution has been retained :

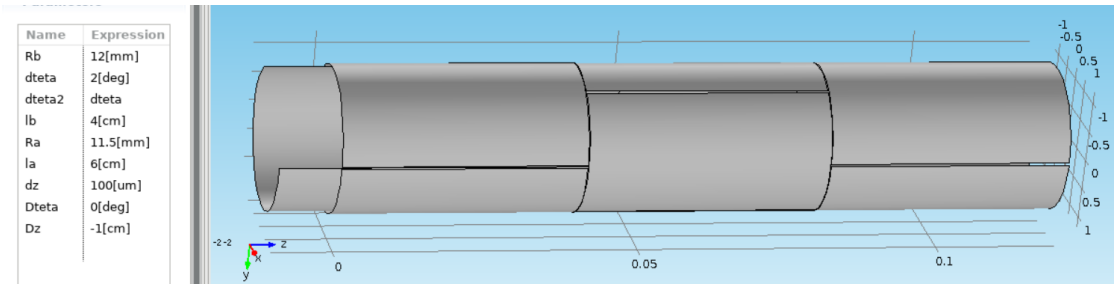

Figure 4.11: Updated solution

This is almost the same prototype, excepted that two modifications have been done:

- One out of two triplets has been shifted by an angle of 60 [°].
- The inner electrode has been extended to a length $l_a = \frac{3}{2} l_b$ in order to always be facing at least 2 triplets.
- In order to keep the same working range, it has also been updated : $\Delta_z = [-\frac{d_{tot}}{2} + \frac{l_a}{3}; \frac{d_{tot}}{2} - \frac{l_a}{3}]$

The 2 algorithms proposed above will be based on the exactly same functioning excepted 1 change (the algorithm based on the look-up table will remain the same). Until now, the θ position was computed using the 3 capacitances having the most facing area with the outer electrodes. Now, in addition to this guessed angle θ_1, an angle θ_2 will also be computed using the capacitances measured on the adjacent triplet that has been shifted by 60 [°]. It will then follow this reasoning :

- If the guessed angle θ_1 belongs to the intervals : $[30, 90][°], [150, 210][°]$ or $[270, 330][°]$. The output angle θ will be equal to θ_1.
- If the guessed angle θ_1 belongs to the intervals : $[0, 30][°], [90, 150][°], [210, 270][°]$ or $[330, 360][°]$. The output angle θ will be taken on the adjacent triplet and therefore be equal to θ_2.

This switching zone is shown on figure 4.12 :

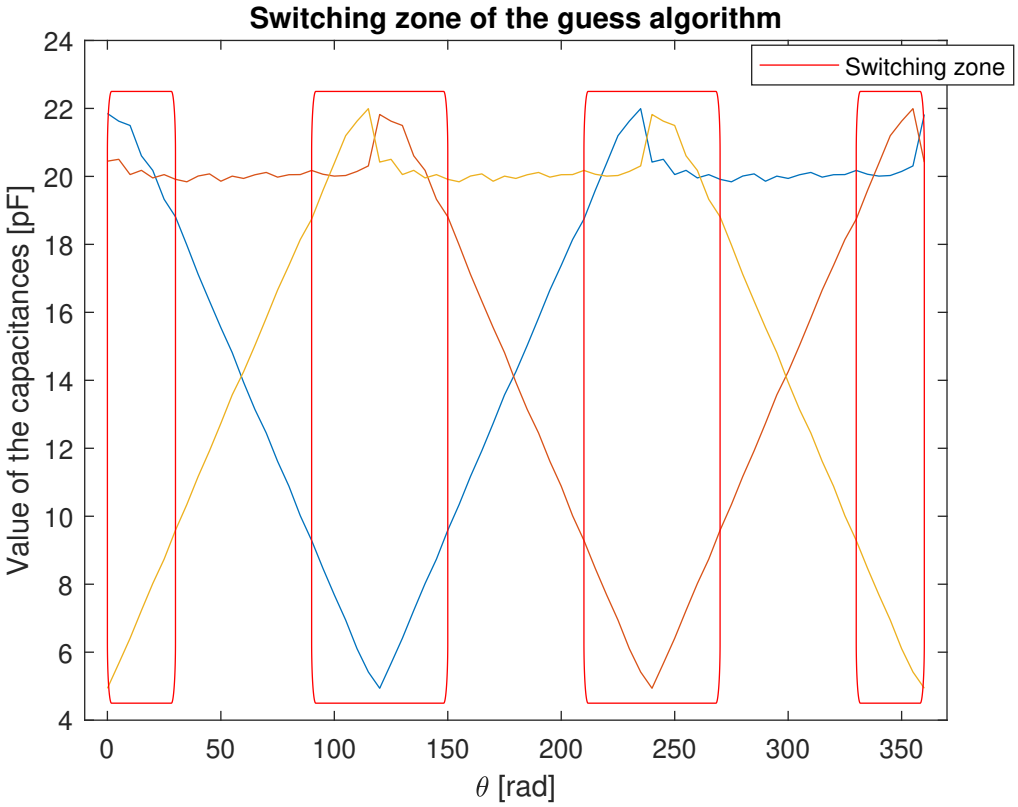

Figure 4.12: Switching zone of the guess algorithm

4.4.1 Results

Using this updated prototype, the following results have been obtained :

Reviewed initial algorithm :

z precision					
Minimum error		Maximum error		Average error	
$3.74e^{-4}$ $[mm]$	$4.7e^{-4}$ [%]	1.04 $[mm]$	1.30 [%]	0.28 $[mm]$	0.35 [%]

θ precision					
Minimum error		Maximum error		Average error	
$2.4e^{-3}$ [°]	$6.68e^{-4}$ [%]	6.07 [°]	1.69 [%]	1.26 [°]	0.35 [%]

Look-up table alogrithm :

z precision					
Minimum error		Maximum error		Average error	
2.84e^{-4} $[mm]$	3.55e^{-4} [%]	0.94 $[mm]$	1.18 [%]	0.16 $[mm]$	0.2 [%]

θ precision					
Minimum error		Maximum error		Average error	
0 [°]	0 [%]	5.88 [°]	1.63 [%]	1.11 [°]	0.30 [%]

Interpolation algorithm :

z precision					
Minimum error		Maximum error		Average error	
3.74e^{-4} $[mm]$	4.7e^{-4} [%]	1.04 $[mm]$	1.30 [%]	0.28 $[mm]$	0.35 [%]

θ precision					
Minimum error		Maximum error		Average error	
5.9e^{-5} [°]	1.41e^{-5} [%]	8.94 [°]	2.49 [%]	2.01 [°]	0.56 [%]

As shown on the results, the modification of the prototype has allowed to reduce the general average error on θ but more importantly to reduce the maximum error. For the first algorithm for example, the maximum error has been reduced from 44 [°] to 6[°]. This has also allowed to obtain an average error which is almost under 0.5% for the 3 algorithms and thus fulfill the expected requirements. This has been achieved while keeping the same average error on the z position.

Chapter 5

Experimental validation of the sensor

In this last chapter, an experimental prototype of the sensor studied all along this paper will be proposed. The different mechanical and electrical components of this prototype will be described and this section will be concluded by presenting the obtained results.

5.1 General description

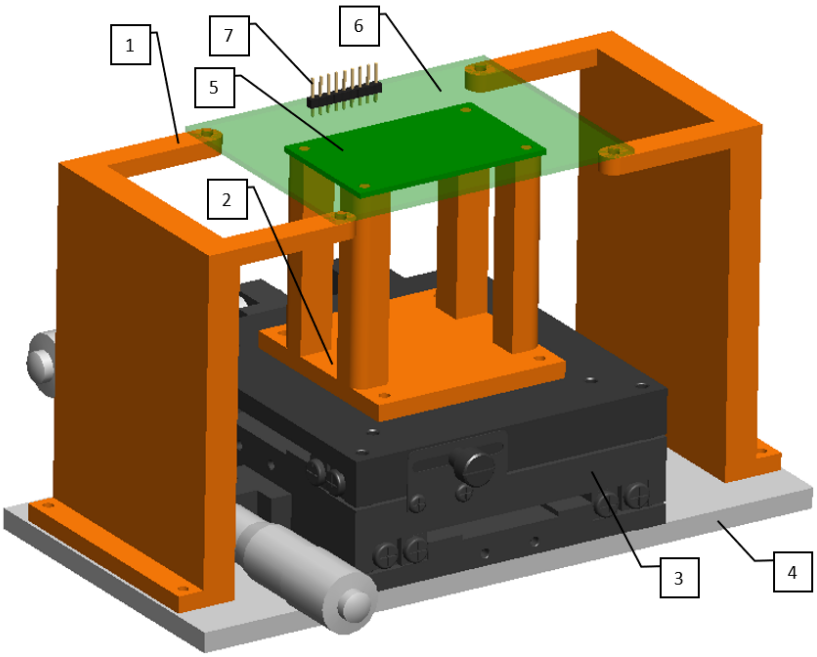

To facilitate his implementation, the cylindrical sensor has been transposed into a 2-D similar working sensor. It is composed of several parts. The rotor's electrode has been replaced by a rigid PCB containing a copper zone (5). This PCB stands on a 3D printed part (2) fixed on two measurements cross rollers (3). This 3D printed part is used to hold the PCB as far as possible from the 2 metalic cross rollers and avoid the interferences that could occur with it when measuring the capacitances. Those 2 measurements cross rollers will make it possible to move the PCB in the x and y direction as they are fixed perpendicularly but also to read the position of this PCB as they are equipped with micrometers. The triplets of electrodes have been replaced by a second PCB containing different copper zones (6). This PCB is fixed with 2 printed parts (1) on a base (4) on which the 2 cross rollers are fixed too. Finally, a 9-Pin header (7) will allow the measurement of the capacitances. To compute the position, a Raspberry PI will be used. It will modify the measured capacitance by controlling multiplexers at a constant rate and read the corresponding capacitance that has been transduced into a voltage.

5.2 Mechanical parts

The 2 cross rollers used in the prototype (figure 5.1) come from Misumi, an online store selling various mechanical components. They have a size of 10x10 [cm] and allow a travel distance of 25 [mm] with a precision of 1 [μm].

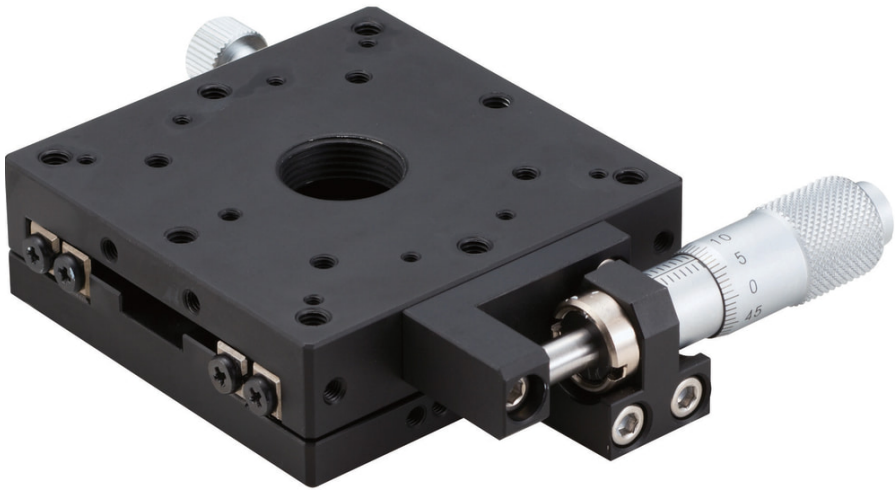

Figure 5.1: Misumi cross rollers

Then the 3D printed part have been realized using the Cetus 3D Printer MK3. The base is made of wood and the different holes have been made using a laser cutting machine to ensure the precision of the positioning of the different parts.

5.3 Electrical parts

In the electrical parts, 3 sections will be considered, the modelisation of the 2 PCBs, the electrical circuit used to complete the measurement of the capacitances and the circuit used to change the measured capacitance.

5.3.1 PCB modelisation

As the 2 cross rollers only allow a displacement range of 25 [mm], the lenght of the copper zones of the fixed PCB have been fixed to $l_b = 16[mm]$ and therefore l_a to $\frac{3}{2}l_b = 24[mm]$. Then, as the electrodes are not cylindrical, their angle of revolution of $\frac{2\pi}{3}$ for the outer electrodes and $\frac{4\pi}{3}$ for the inner electrode have been replaced by electrodes of a width respectively equal to 24 and 48 [mm]. Finally, smaller copper zones have been added at the extremity of the fixed PCB to ensure the continuity of the electrodes in the θ direction as it is the case in the 3D configuration.

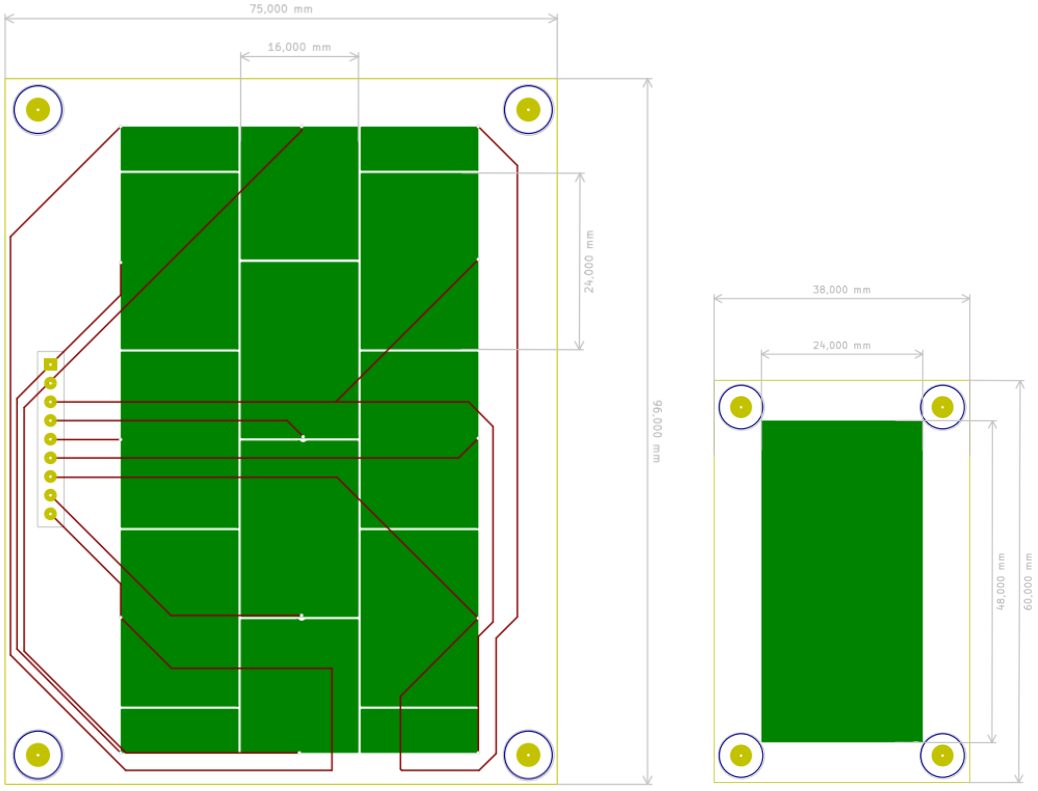

(a) Fixed PCB modelisation

(b) Moving PCB modelisation

Figure 5.2: PCB design

5.3.2 General circuit

The circuit used to complete the measurements is the following :

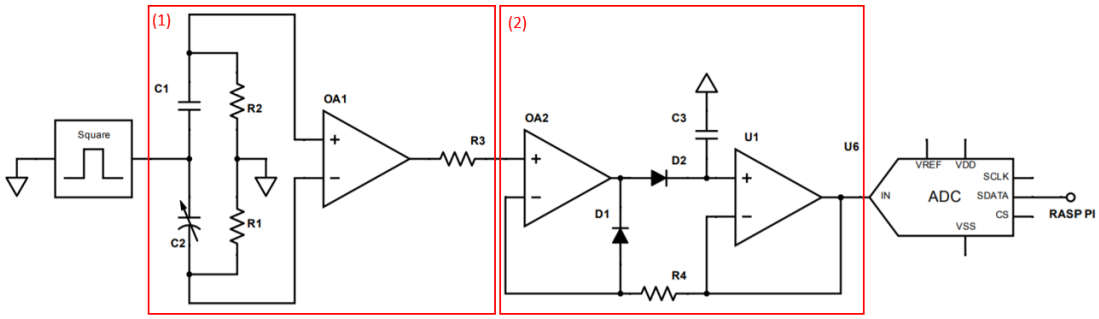

Figure 5.3: Measurement circuit

It is composed of 5 parts :

- A square voltage source with a given frequency f and voltage V.
- An alternating current bridge followed by a comparator OP amp (1).
- A peak detector circuit (2).
- An analog-to-digital converter.
- A raspberry PI.

It works as follows :

The voltage source, alternating current bridge and OP amp together, will give as ouput signal a square wave with a peak value depending on the measured capacitances C_2. The peak detector will then only keep the DC peak value of this square signal. Finally, the analog-to-digital will convert the output voltage into a readable signal for the raspberry PI. The converter used in this prototype is the ADS1115 that is capable of measuring voltage in a working range 2-5 [V]. The circuit will therefore be designed in a way to have the largest possible output voltage range within this working range.

To do so, the first step was to know the typical values of the measured capacitances. A Comsol model have therefore been established with the prototype parameters and the returned values of capacitances were in the range $[1.5, 4.5]$ $[pF]$. Knowing this, the circuit have been designed with the following parameters :

- A square wave with V between 0 and 2 [V] and a frequency $f = 1$ $[kHz]$ that will be generated by a picoscope

- $C_1 = 4\ [pF]$
- $R_1 = 12\ [k\Omega]$
- $R_2 = 6\ [k\Omega]$
- $R_3 = 1\ [k\Omega]$
- The OP amp. OA1 is a MCP6292 supplied with $V_+ = 5\ [V]$ and $V_- = 0\ [V]$
- The OP amp. of the peak detector are TL084CN powered with $V_+ = 15\ [V]$ and $V_- = -15\ [V]$
- $R_4 = 10\ [k\Omega]$
- $C_3 = 5\ [nF]$

This circuit has been tested with the software LTspice to verify its working.As constant output voltages between 2.5 and 4.75 [V] have been obtained, the parameters of the circuit have been validated. The output of the comparator OP amp. and the peak detector are shown on figure 5.4.

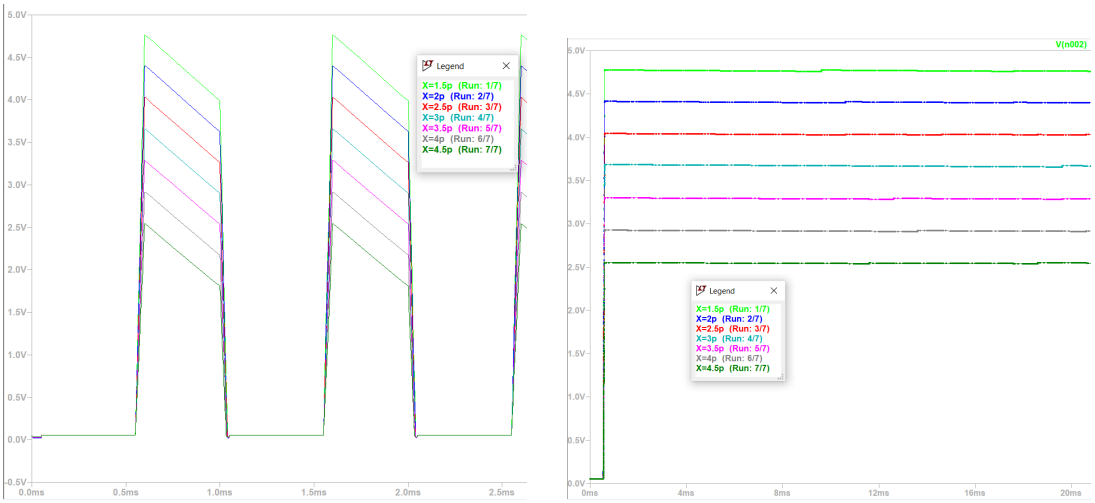

(a) Comparator OP amp. output

(b) Peak detector output

Figure 5.4: LTspice outputs

5.3.3 Choice of the measured capacitance

To choose the capacitance that will be measured by the circuit, analog multiplexers will be used. Multiplexers are data selectors that allow to change the output signal that will be chosen between n input signals depending on the binary code that has been sent to it. As 9 different capacitances are being measured, two 8:1 and two 2:1 multiplexers will be needed. The corresponding circuit with its truth table is shown on figure 5.2. In this circuit, the 9 inputs C_1 to C_9 correspond to the 9 electrodes of the fixed PCB and the output will replace the variable capacitance C_2 in the measuring circuit presented above. The signals A,B,C and D will be sent by the GPIO's output of the Raspberry PI and set to HIGH or LOW in order to choose the desired measured capacitance. Pratically, 4 multiplexers CD74HC4051E from Texas Instrument have been chosen. These are 8:1 analog multiplexers working in the range 0-5 [V] and as 2 of them have to be used as 2:1 multiplexers, 3 of the 4 selection input signals have been fixed to 0 [V].

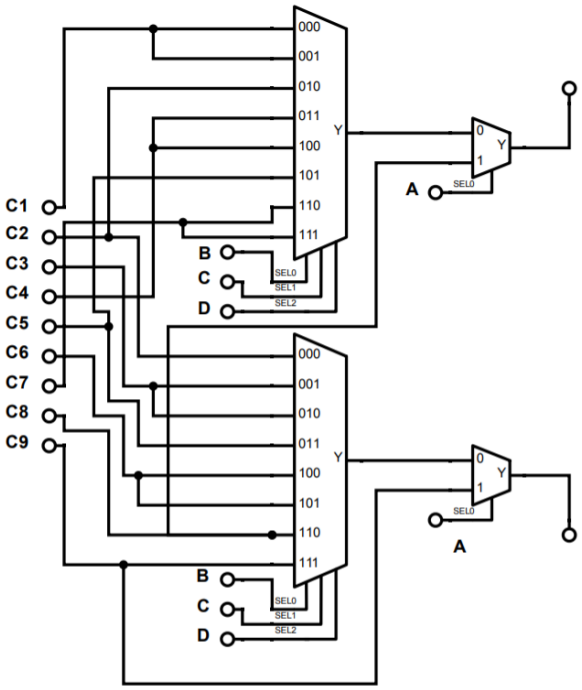

Table 5.1: Multiplexer circuit

A	B	C	D	**Y**
0	0	0	0	**C12**
0	0	0	1	**C13**
0	0	1	0	**C23**
0	0	1	1	**C45**
0	1	0	0	**C46**
0	1	0	1	**C56**
0	1	1	0	**C78**
0	1	1	1	**C79**
1	x	x	x	**C89**

Table 5.2: Corresponding truth table

5.4 Results

The achieved prototype is shown on figure 5.5

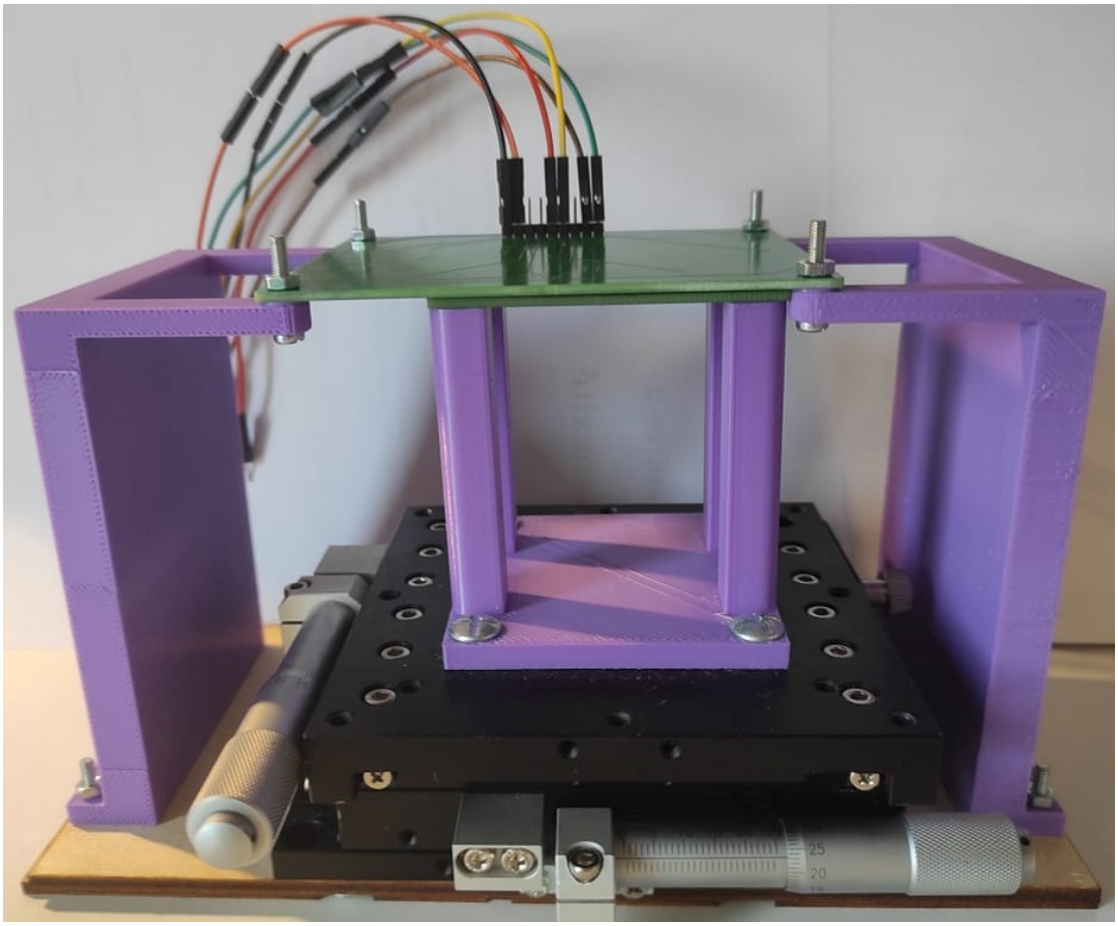

Figure 5.5: Achieved prototype

Firstly, the correct functioning of the measurement circuit has been verified by displaying the output of the comparator OP amp. and the peak detector using a picoscope. The corresponding signals are shown on figure 5.6 with in red the output of the OP amp. and in blue the output of the peak detector.

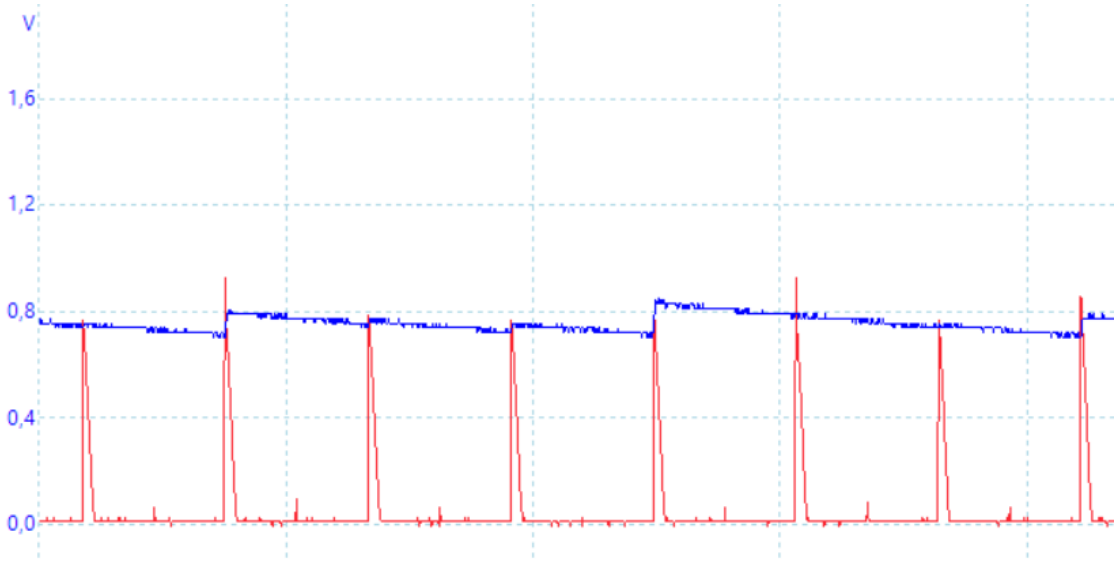

Figure 5.6: Measured output signals

As the output of the peak detector wasn't as constant as expected, the frequency of the square wave signal have been increased to 5 $[kHz]$. This leads to a much steadier signal (figure 5.7)

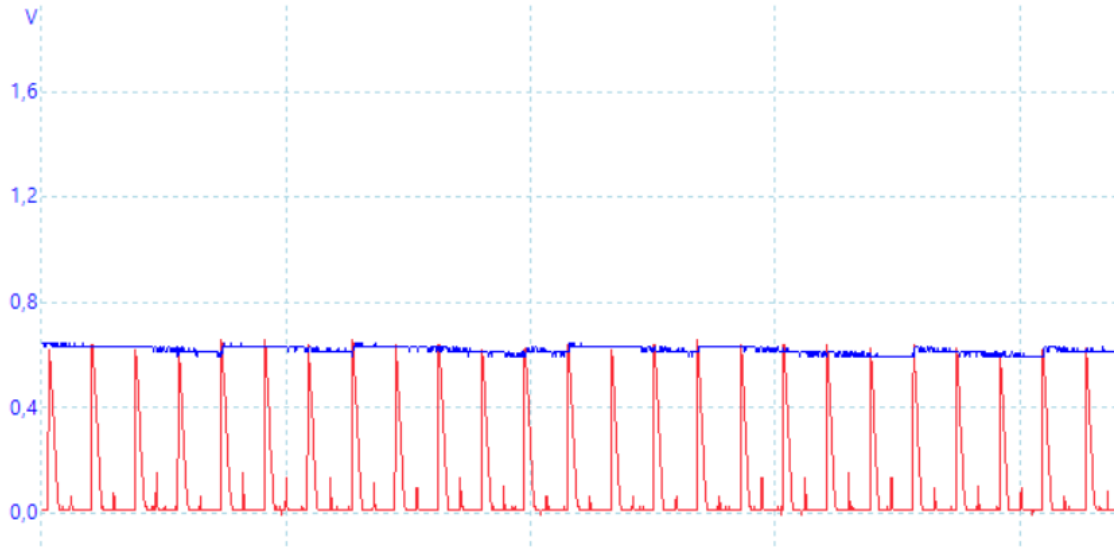

Figure 5.7: Measured output signal with increased frequency

In addition to this, the displaying of the output signals has also revealed a difference in the expected range of measured voltage. Indeed, this output was in the interval [0.6;2] [V] which is almost 2 times smaller than the expected range. This has

been explained by the fact that the measured capacitances are different from those computed by Comsol. However the first algorithm has been tested on the prototype for two different displacements of 24 [mm] (one along the x axis and the other along the y axis) in order to characterize its precision. The measurements have been done according the following procedure :

- The selection signals sent to the multiplexers are changed every 0.2 [s] in order to measure the 9 capacitances in a period of less than 2 [s].
- The position is computed using the 9 measured capacitances and stored in a list.
- Once the position is computed, a message is printed and the function is suspended during 5 [s] allowing the user to modify the position of the electrode using the micrometric rollers.
- The previous steps are repeated a fixed number of times and finally, the list containing the positions is written in a .txt file.

As 24 [mm] corresponds to a displacement in the range $[0, 120]$ ° in the θ direction and $[-12, 12]$ $[mm]$ in the z direction, the following results have been obtained by measuring 49 positions in each direction (1 every 0.5 [mm]) :

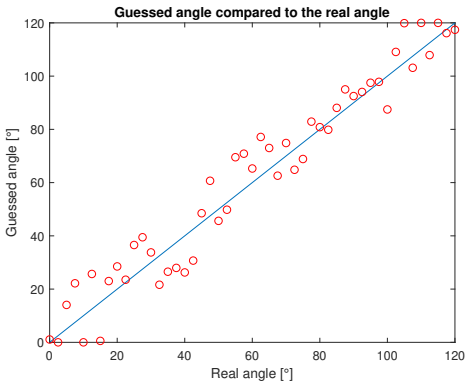

(a) Error on the θ position

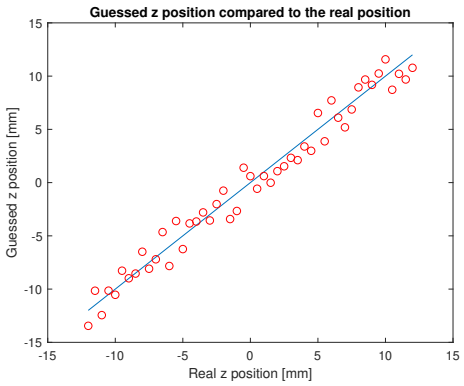

(b) Error on the z position

Figure 5.8: Measurement error on the position

z precision					
Minimum error		Maximum error		Average error	
0.015 [mm]	0.06 [%]	1.92 $[mm]$	8 [%]	1.07 $[mm]$	4.47 [%]

θ precision					
Minimum error		Maximum error		Average error	
0.35 [°]	0.10 [%]	14.9 [°]	4.13 [%]	7.21 [°]	2.0 [%]

As those results are acceptable, they are relatively far from the expected precision but this can be justified by the following non-idealities and differences compared to the considered model:

- The prototype is a 2-D representation of the sensor. The interactions between the electrodes could therefore not be exactely the same.
- As the electrodes are placed in a PCB made of various materials, the relative permittivity is not equal to 1 everywhere.
- The 2 PCBs are not perfectly parallel to each other due to the imprecision of the 3D printed parts.
- Electrical noises due to the OP amps, measuring wires and multiplexers that are hardly predictable.
- Unprecision due to the analog-to-digital converter
- Noises due to the square signal generated by the picoscope.

The following list of track of improvements has therefore been established in order to try to fix those non-idealities:

- Use of manufactured parts instead of 3D printed to reduce the distance unprecision between the PCBs.
- Use of PCBs instead of a breadboard for the rest of the circuit in order to reduce the noises coming from the large number of wires.
- Use of a more reliable voltage source.
- Use of a more efficient and accurate voltage measurement device.

Chapter 6

Conclusion

In this paper, the complete study and design of a 2 degree-of-freedom capacitive sensor has been achieved. The prototype has been first presented in chapter 1 with its general concept and functioning. In chapter 2, the sensor has been first tested considering an ideal case. Then an analytical model has been developped in order to analyze the impact of the different parameters on the functioning of the sensor. Further, in chapter 3, an other approach has been taken by studying the model using a finite element method. This has allowed to highlight non-idealities that could not easily be taken into account with an analytical approach. In chapter 4, 3 algorithms have been developed trying to handle those non-idealities by using different methods of measurement. It has also allowed to realize that the prototype had to be updated in order the fulfill the desired precision requirements. Finally, an experimental prototype has been made in order to discuss the results described throughout this paper.

More precisely, it has allowed to realize the difficulties encountered when moving from theory to practice but also to demonstrate that it is almost impossible to consider and predict all the non-idealities brought by the various physical interactions of the environment.

However, even if the prototype is still far from its final version, this paper has allowed to validate its general concept of functioning and to highlight the different track of improvement that could be performed on the sensor in order to overcome the precision issues.

Bibliography

[1] Misumi - configurable mechanical components, https://uk.misumi-ec.com/vona2/detail/110300196460/?PNSearch=XPG100&HissuCode=XPG100&searchFlow=suggest2products&Keyword=XPG100#

[2] Cetus - 3D printer,https://shop.tiertime.com/product/cetus-3d-printer-mk3/

[3] Fanuc - The factory automation company,https://www.fanuc.eu/be/nl/robots/robot-filter-pagina/scara-series/scara-sr-3ia

[4] Alireza Mohammadi,H.J. Marquez,Mahdi Tavakoli. *"Disturbance Observer-based Trajectory Following Control of Nonlinear Robotic Manipulators"* June 2011.

[5] Louis BODY,Martin VAN ESSCHE *"Design, optimization and realization of a two-degree-of-freedom permanent magnet actuator"*,2019.

[6] Alan Kardek Rêgo Segundo,José Helvecio Martins,Paulo Marcos de Barros Monteiro,Rrubens A. de Oliveira,Delly Oliveira Filho. *"Development of capacitive sensor for measuring soil water content"* April 2011.

[7] A. S. Anil Kumar, Narendiran Anandan,Boby GeorgeSubhas Chandra Mukhopadhyay, *"Improved Capacitive Sensor for Combined Angular and Linear Displacement Sensing"* November 2019.

[8] DesignWorld,https://www.designworldonline.com/what-is-the-difference-between-an-absolute-and-incremental-position-encoder/

[9] EEEGUIDECOM - Online electrical and Electronics Study,https://www.eeeguide.com/types-of-encoders-in-digital-electronics/

[10] Wikipedia - De Bruijn sequence,https://en.wikipedia.org/wiki/De_Bruijn_sequence

[11] Wikipedia - De Bruijn sequence,https://en.wikipedia.org/wiki/De_Bruijn_sequence

[12] EMI - software,https://www.emisoftware.com/calculator/coplanar-capacitance/

[13] Comsol,https://www.comsol.com/

[14] Electronics Coach,https://electronicscoach.com/peak-detector.html

UNIVERSITÉ CATHOLIQUE DE LOUVAIN
École polytechnique de Louvain
Rue Archimède, 1 bte L6.11.01, 1348 Louvain-la-Neuve, Belgique | **www.uclouvain.be/epl**